Award Accounts

The Chemical Society of Japan Award for Creative Work for 2009

Toward an Atomic-Level Understanding of Size-Specific Properties of Protected and Stabilized Gold Clusters

Tatsuya Tsukuda

Catalysis Research Center, Hokkaido University, Nishi 10, Kita 21, Sapporo, Hokkaido 001-0021

Received July 29, 2011; E-mail: tsukuda@cat.hokudai.ac.jp

Metal clusters consisting of fewer than 100 atoms (diameter <2 nm) are highly promising as a new class of building units for functional materials because of their novel and size-dependent properties. Nevertheless, basic and applied studies of metals clusters have been hampered by the lack of specific guidelines for design and precise synthetic methods. This account surveys recent investigations of gold clusters focusing on our effort toward an atomic-level understanding and control of their size-specific properties. We have developed a size-controlled method for synthesizing gold clusters protected by ligands, stabilized by polymers, and supported on solids. Remarkable size-effects on stabilities and various properties including catalysis were observed. Their mechanisms are discussed based on fundamental knowledge of bare gold clusters in the gas phase.

1. Introduction

Over the past few decades, metal nanoparticles (MNPs) with diameters smaller than 100 nm have attracted much interest as a new metallic state because their small sizes cause their thermodynamic, electrical, magnetic, chemical, and optical properties to differ from those of their corresponding bulk metal. For example, the liquid-drop model predicts that the ionization potentials, electron affinities, and melting temperatures of MNPs will all vary with diameter.[1] In other words, the properties of MNPs can be scaled from those of the corresponding bulk metal. The scaling laws provide a design principle for MNPs with tailored properties for specific applications.

In contrast, metal clusters (MCLs) composed of fewer than 100 atoms (diameter <2 nm) exhibit novel properties that differ greatly from those predicted by simple scaling laws.[2] The nonscalable nature of MCLs is ascribed to their quantized electronic structures and unique geometrical structures (e.g., the formation of icosahedral motifs). Another attractive feature of MCLs is that their properties can be tuned over a wide range by varying the number of constituent atoms (i.e., the *cluster size*).[2] Because of these unique features, the MCLs are promising candidates for functional units or building blocks of novel materials. The goal of our research is to develop novel materials by exploiting these unique characteristics of MCLs based on a rational principle (Figure 1). To realize this goal, it is necessary to stabilize MCLs against aggregation because their high surface energies make them extremely unstable. Several methods have been used to stabilize MCLs. Complete passivation of the cluster surface by organic ligands enables them to be manipulated as conventional chemical compounds. Introducing functional groups into such ligands will expand the range of their applications of MCLs. Partial passivation of the cluster surface by polymers or immobilization on solids is ideal for catalytic applications since the exposed areas of the clusters can be used for catalytic conversion. To optimize the properties of MCLs, it is necessary to control the cluster size over a certain range with an atomic resolution. However, precise synthesis of MCLs is technically challenging.

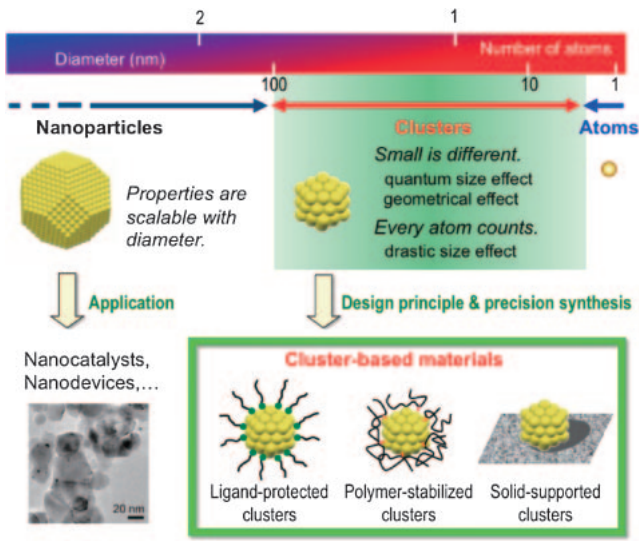

Figure 1. Concept for the development of cluster-based materials.

Published on the web February 10, 2012; doi:10.1246/bcsj.20110227

A rational design principle is required to develop cluster-based materials to avoid trial-and-error screening of a wide range of parameters, including constituent elements, size, and structure of MCLs. Gold clusters (AuCLs) were chosen as the initial target of our research because guides for their stability and various properties have been established by extensive experimental and theoretical studies of bare AuCLs isolated in the gas phase.[3–6] For example, the high stability of Au_n with $n = 8$, 18, 20, 34, 58, ... (magic numbers) can be explained by the electronic-shell model in which delocalized valence electrons occupy shells in a spherical jellium potential.[3–6] The discovery of the catalysis of gold nanoparticles (AuNPs) by Haruta and co-workers[7] has convinced us that AuCLs can act as efficient oxidation catalysts. In addition, formation of superoxo or peroxo species on small AuCLs in the reaction with O_2 (Refs. 8–12) hints at the possibility that they could catalyze aerobic oxidation, which is currently of interest from the viewpoint of green chemistry. Experiments have demonstrated that CO can be catalytically oxidized to CO_2 by O_2 using AuCLs isolated in the gas phase[8,12] or anchored on a well-defined metal oxide surface.[13]

The present paper summarizes our study of size-selective synthesis of AuCLs and their size-specific properties. Section **2** discusses AuCLs protected by organic ligands such as thiolates (RS^-) and phosphines (PR_3). Our synthetic method allowed us to discover a series of magic AuCLs. We propose a simple building-up principle for magic thiolated AuCLs. Some unique properties of a prototype magic cluster $Au_{25}(SR)_{18}$ are summarized. Sections **3** and **4** describe size-controlled preparation of AuCLs stabilized by a hydrophilic polymer and anchored on solids, respectively. To focus on the size dependence on the intrinsic catalytic properties of AuCLs, we chose poly(*N*-vinyl-2-pyrrolidone) (PVP) as a polymer and mesoporous silica (SBA-15) and hydroxyapatite (HAP) as solid supports since they are chemically inert and do not directly participate in oxidation catalysis. Remarkable size effects were observed for the oxidation reactions of alcohols, styrene, and cyclohexane using molecular oxygen as an oxidant. An aerobic oxidation mechanism was proposed based on O_2 activation by AuCLs, which is also the key process in the oxidation by model Au catalysts.[8–13] Finally, Section **5** summarizes our work and discusses future prospects.

2. Ligand-Protected Au Clusters

2.1 Size-Controlled Synthesis. 2.1.1 Strategy: Thiolates (RS^-) and phosphines (PR_3) were employed as protecting ligands for the AuCLs[14–19] due to the high affinities of sulfur and phosphorus for gold. A basic strategy for synthesizing a series of ligand-protected AuCLs with well-defined formulas consists of three steps (Figure 2). The first step is wet-chemical preparation of crude mixtures of clusters. They are then fractionated by size by extraction, chromatography, or electrophoresis. Finally, mass spectrometry is used to determine the formulas of fractionated clusters. Some details of each step are described below.

2.1.2 Chemical Preparation of Crude Mixtures: Crude mixtures of AuCLs protected by thiolates and phosphines were prepared by reducing Au ions complexed with the corresponding ligands by $NaBH_4$ as shown in Figure 2.[14–19]

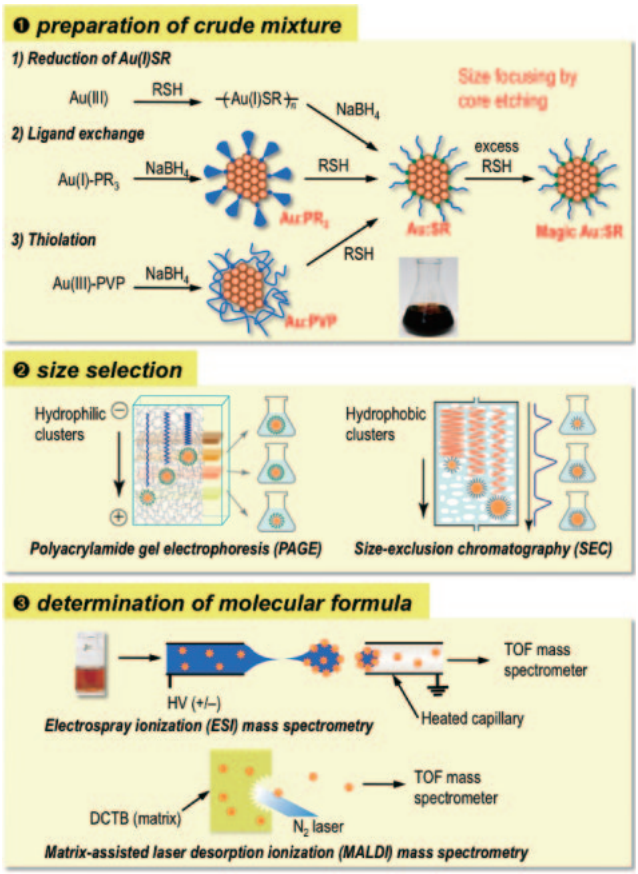

Figure 2. Experimental procedure for size-selective synthesis of ligand-protected AuCLs.

$$[Au^{III}Cl_4]^- \xrightarrow{RSH} Au^I{:}SR \xrightarrow{NaBH_4} Au^0{:}SR \quad (1)$$

$$Au^IX \xrightarrow{PR_3} Au^I{:}PR_3 \xrightarrow{NaBH_4} Au^0{:}PR_3 \quad (2)$$

Reaction (1) includes the Brust method.[14] To prepare small clusters, the relative ratio of the ligand to Au was increased and the reaction temperature was reduced. By exploiting the very strong Au–S interaction, Au:SR clusters were also prepared by the following two methods: ligand-exchange reaction[20–22] of $Au{:}PR_3$ and thiolation of Au:PVP.

$$Au^0{:}PR_3 \xrightarrow{RSH} Au^0{:}SR \quad (3)$$

$$Au^0{:}PVP \xrightarrow{RSH} Au^0{:}SR \quad (4)$$

The AuCLs obtained after purification were brownish and did not exhibit surface plasmon resonance absorption. Transmission electron microscopy (TEM) showed that the Au cores had diameters smaller than 2 nm.

2.1.3 Size Selection: The crude mixtures of the AuCLs were size fractionated by solvent extraction since the dispersibility of the clusters in a liquid medium depends on their core mass.[15,16] $[Au_{11}(PPh_3)_8Cl_2]^+$, $[Au_{11}(BINAP)_4X_2]^+$,[23] and $[Au_{25}(PPh_3)_{10}(SC_nH_{2n+1})_5Cl_2]^{2+}$ (Ref. 24) were successfully isolated by gradually varying the polarity of the solvent.

However, since fractional extraction requires trial-and-error testing, a more straightforward and reproducible method is desired. Au:SR consists of AuCLs protected by a robust

monolayer with a uniform thickness. This enables as-prepared Au:SR to be fractionated based on their total size using polyacrylamide gel electrophoresis (PAGE)[25–31] or size exclusion chromatography (SEC: Figure 2).[32–34] Larger molecules generally take more time to pass through the gel than smaller ones in PAGE, whereas larger molecules elute faster than smaller ones from a porous hydrophobic microgel in SEC. However, these conventional methods had to be adapted for Au:SR since core sizes of different Au:SR differ by a few Au atoms to a few tens of Au atoms. The resolution of PAGE separation was significantly improved by employing gels that were much denser than conventional gels used for protein separation. The SEC resolution was enhanced by employing a recycling SEC system in which Au:SR was allowed to repeatedly pass through the column. Typically, about 2 and 10 mg of isolated Au:SR were obtained by PAGE and SEC, respectively; these quantities are sufficient for most characterizations.

2.1.4 Molecular Formula Determination: The chemical compositions of the fractionated AuCLs were investigated by mass spectrometry. In the initial stages of the research, laser desorption ionization (LDI) was frequently used for this purpose.[15,16,21,32,33,35–38] However, this provided only an approximated estimate of the core mass of Au:SR because the LDI process breaks C–S bonds and probably Au–Au bonds, resulting in the formation of fragments with the formula Au_nS_m. We utilized two methods to suppress fragmentation: electrospray ionization (ESI)[22–28,30,39–49] and matrix-assisted LDI (MALDI).[34,49–52]

Both hydrophilic and hydrophobic AuCLs were studied using a homemade ESI mass spectrometer by respectively exploiting the electronic charges of the functional groups of the ligands and those of the Au core imparted by redox reactions (Figure 2). The dispersion was delivered by a syringe pump and electrosprayed through a stainless-steel needle of a syringe biased at ca. −3 kV into a grounded capillary positioned in a coaxial configuration. The central part of the sprayed cone, which contained large droplets, was fed into a resistively heated capillary to promote desolvation. At an optimized capillary temperature, the solvents are efficiently evaporated from the droplets so that only desolvated intact cluster ions were formed. MALDI mass analysis of Au:SR was conducted using a commercially available system (Voyager-DE STR-H, Applied Biosystems); the samples were mixed with *trans*-2-[3-(4-*tert*-butylphenyl)-2-methyl-2-propenylidene]malononitrile (DCTB)[50] and irradiated with a N_2 laser (337 nm). Under an optimized mixing ratio of Au:SR and DCTB and optimal laser fluence, Au:SR was ionized in the intact form and detected by a time-of-flight mass spectrometer.

2.2 Thiolate-Protected Au Clusters. 2.2.1 Magic Clusters: Free AuCLs with 8, 18, 20, 34, 58, … valence electrons are much more stable than AuCLs with similar but different numbers of valence electrons: consequently, they are referred to as magic clusters.[3–6] An interesting and fundamental question is: what are the magic clusters for Au:SR?[15–17] Whetten was the first to isolate a series of stable Au:SR clusters by treating them as conventional chemical compounds and found magic clusters with core masses of ca. 8, 14, 22, and 29 kDa by LDI mass spectrometry.[15,16] In 2005, we reported the first size-selective synthesis of Au:SR clusters with

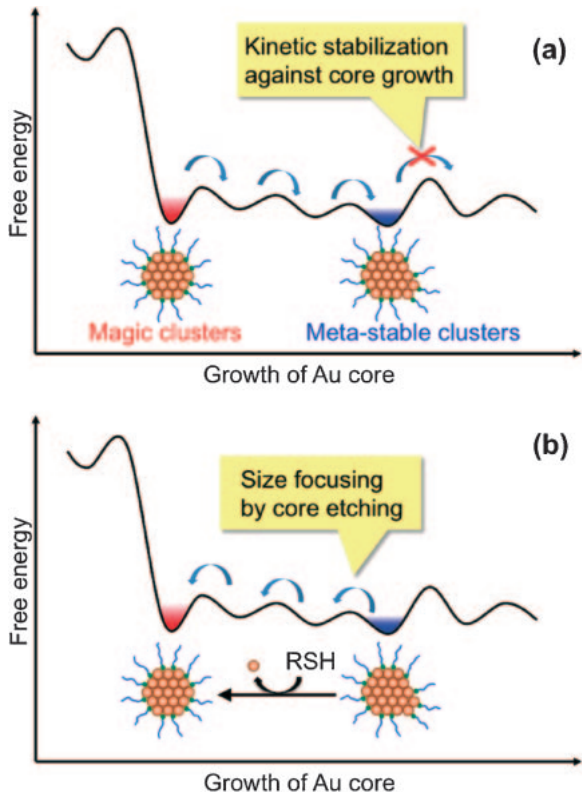

Figure 3. (a) Kinetic stabilization and (b) chemical etching of Au core.

well-defined chemical formulas of $Au_{10}(SG)_{10}$, $Au_{15}(SG)_{13}$, $Au_{18}(SG)_{14}$, $Au_{22}(SG)_{16}$, $Au_{22}(SG)_{17}$, $Au_{25}(SG)_{18}$, $Au_{29}(SG)_{20}$, $Au_{33}(SG)_{22}$, and $Au_{39}(SG)_{24}$ (where SG represents glutathionate).[28] At that time we considered these clusters to be a series of magic clusters. However, their stabilities were found to depend on their core sizes; $Au_{18}(SG)_{14}$, $Au_{25}(SG)_{18}$, and $Au_{39}(SG)_{24}$ were more stable than the other clusters when stored in an aqueous solution.[28] This finding suggested that Au:SR clusters isolated from the crude mixture produced by reaction (1) do not always correspond to magic clusters. This idea was supported by the observation that the sequence of core sizes of the isolated clusters depends on the structure of the thiolates[30] and differs from those expected from the closed electronic or geometric structures of free AuCLs.

The above conclusion can be explained by assuming that reaction (1) yields magic Au:SR clusters as well as metastable clusters that are kinetically stabilized during the reduction of $Au^{I}SR$ polymers. As depicted schematically in Figure 3, Au cluster growth proceeds irreversibly and there is strong competition with surface protection by thiolates. Under such circumstances, consecutive core growth is kinetically hindered during stages in which the core is completely protected by the thiolate ligand shell (Figure 3a). The stage at which growth is terminated may be determined from the molecular structures of the thiolates and/or the probability of ligation of the thiolates. How can we distinguish the magic clusters from the series of isolated clusters? We showed that the cores of metastable clusters can be selectively etched by excess thiols[53] to form magic clusters (Figure 3b). For example, $Au_{25}(SG)_{18}$ was extremely stable in the presence of excess GSH, whereas

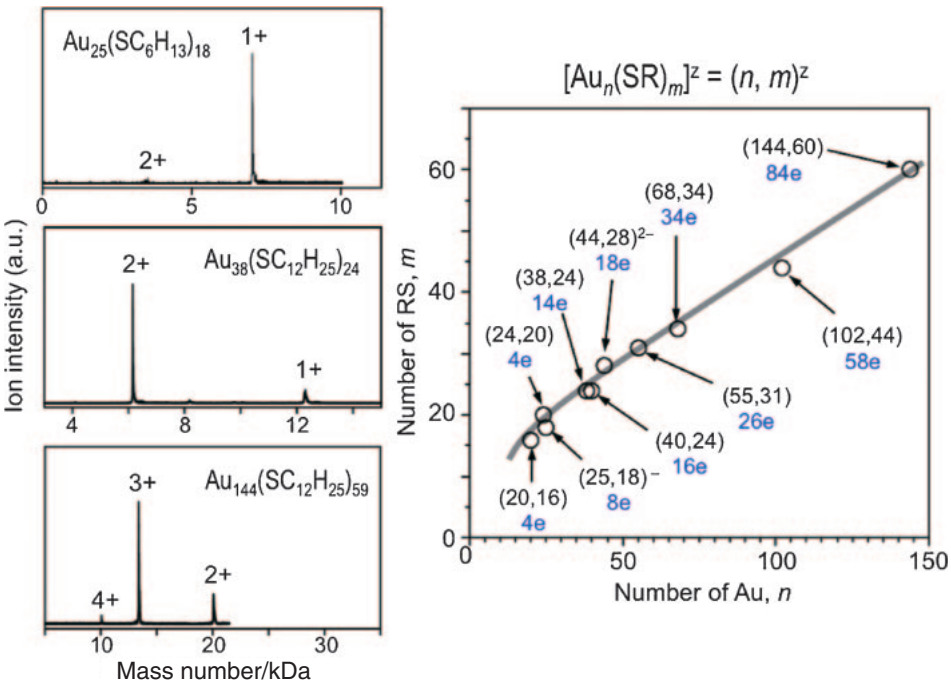

Figure 4. Examples of ESI mass spectra (left) and chemical compositions of magic Au:SR clusters reported so far (right). The blue numbers represent the numbers of valence electrons obtained using eq 5. The line is a guide for the eye.

$Au_n(SG)_m$ ($39 > n > 25$) and $Au_n(SG)_m$ ($n < 25$) were respectively transformed into $Au_{25}(SG)_{18}$ and Au^I:SG complexes under the same conditions.[53] This observation indicates that the Au core of metastable $Au_n(SG)_m$ ($39 > n > 25$) is etched by free GSH into $Au_{25}(SG)_{18}$, which is extremely stable against etching. By exploiting this size-specific stability, we achieved a large-scale, selective production of $Au_{25}(SG)_{18}$.[22] Based on these results, we conclude that $Au_{25}(SR)_{18}$ is the smallest member of a family of magic Au:SR clusters.[28]

These results indicate that the stability of the clusters against size reduction caused by processes such as chemical etching should be studied to determine a series of magic core sizes out of the Au:SR clusters formed by reaction (1). Size focusing of preformed Au:SR clusters by thiol etching is currently the general approach for size-selective synthesis of magic Au:SR clusters.[33,44,51–56] By using this approach and ESI mass spectrometry, we revealed that Au:SC_n clusters with core masses of 8 and 29 kDa are ubiquitous magic clusters and that they can be formulated as $Au_{38}(SC_n)_{24}$ and $Au_{144}(SC_n)_{59}$, respectively (Figure 4).[43] Murray and Jin later reassigned the latter clusters as $Au_{144}(SC_n)_{60}$,[46,47] which possibly explains our observation that $[Au_{144}(SC_n)_{59}]^{x+}$ is an ESI-induced dissociation of one thiolate from $Au_{144}(SC_n)_{60}$. Recent experimental studies by several groups have established a series of magic Au:SR clusters: $Au_{19}(SR)_{13}$,[57] $Au_{20}(SR)_{16}$,[39] $Au_{24}(SR)_{20}$,[40] $Au_{25}(SR)_{18}$,[22,28,41,42,51,53,55,58–63] $Au_{36}(SR)_{23}$,[64] $Au_{38}(SR)_{24}$,[43,44,56,65–67] $Au_{40}(SR)_{24}$,[45,65] $Au_{44}(SR)_{28}$,[49] $Au_{55}(SR)_{31}$,[34] $Au_{68}(SR)_{34}$,[52] $Au_{102}(SR)_{44}$,[48,68] and $Au_{144}(SR)_{60}$.[46,47,69] Figure 4 shows a plot of the chemical compositions of these magic Au:SR clusters. There is clearly a very strong correlation between the numbers of Au atoms and thiolates; however, the core sizes of the magic Au:SR clusters do not match those of free magic AuCLs.

The ligand-exchange reaction (3)[21] and thiolation reaction (4)[32–34] yielded new magic clusters, which could not be obtained from samples prepared by the conventional Brust method (reaction 1). Murray and co-workers have reported that Au:SC_6 clusters with core masses of ≈11 kDa were formed by the reaction of $Au_{55}(PPh_3)_{12}Cl_6$ with hexanethiol.[21] By thiolation of Au:PVP (reaction 4), we obtained magic Au:SC_{18} clusters with a core mass of 11 kDa.[32] Recent MALDI-MS analysis indicated that the 11-kDa clusters were mainly $Au_{55}(SC_{18}H_{37})_{31}$ with some contamination by $Au_{54}(SC_{18}H_{37})_{30}$.[34] This situation is similar to that in the production of the magic cluster $Au_{38}(SR)_{24}$. The $Au_{38}(SC_{18}H_{37})_{24}$ yield by the Brust method was very low, but it could be significantly increased by thiol etching of larger Au:SC_{18}.[43,44,56] The nonformation of $Au_{38}(SR)_{24}$ and $Au_{55}(SR)_{31}$ by the chemical reduction of Au^ISR oligomers is ascribed to the different kinetics of Au:SR formation.

2.2.2 Origin of Magic Clusters: What is the origin of the high stability of these magic clusters? Magic numbers for AuCLs in the gas phase[3–6] and protected by phosphines, such as $[Au_{11}(PPh_3)_8Cl_2]^+$ and $Au_{11}(PPh_3)_7Cl_3$, can be explained by the electronic shell model: the clusters gain high stability when the total numbers of the valence electrons are 2, 8, 18, 20, 34, … because the electronic shell is closed. To account for the magic stability of $Au_n(SR)_m$, Häkkinen proposed a "superatom concept"[70] in which the $Au_n(SR)_m$ clusters with total numbers of valence electrons (N^*) of 2, 8, 18, 34, 58, 92, … are stable because their electronic structures are closed,

$$N^* = n \times V_A - m - z \quad (5)$$

where n is the number of Au atoms, V_A is the number of valence electrons per Au atom ($V_A = 1$), m is the total charge localized on the ligands, and z is the net charge of the AuCLs.

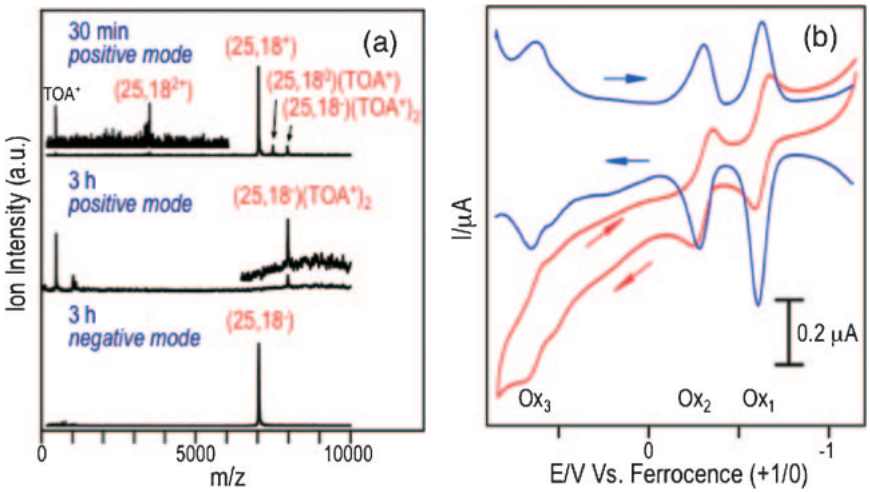

Figure 5. (a) Typical ESI mass spectra of $Au_{25}(SC_6H_{13})_{18}$ obtained by the Brust method after 30 min and 3 h. The notation $(n, m^{-/+})$ represents $[Au_n(SC_6H_{13})_m]^{-/+}$. (b) Superimposed square-wave (blue) and cyclic (red) voltammograms of $Au_{25}(SC_{12}H_{25})_{18}$ in a dichloromethane solution of $TBAPF_6$ in an Ar atmosphere at −20 °C.

The numbers of blue characters in Figure 4 are the n^* values calculated for the magic Au:SR clusters. In many cases, the numbers equal the expected values. For example, the n^* values are 8, 18, 34, and 58 for $[Au_{25}(SR)_{18}]^-$ (Refs. 42, 50, and 60–62), $[Au_{44}(SR)_{28}]^{2-}$ (Ref. 49), $[Au_{68}(SR)_{34}]^0$ (Ref. 52), and $[Au_{102}(SR)_{44}]^0$ (Ref. 68), respectively.

However, there are several exceptions, suggesting that the electronic structure does not solely determine the stability of the magic clusters. Indeed, we demonstrated that $[Au_{25}(SC_6H_{13})_{18}]^x$ can have various charge states depending on the synthesis conditions:[42] this contrasts sharply with the case of phosphine-protected AuCLs, which adopt specific charge states to fulfill the electron counting scheme. Figure 5a shows ESI mass spectra of $[Au_{25}(SC_6H_{13})_{18}]^x$ extracted with acetonitrile after 30 min and 3 h of reaction (1). $[Au_{25}(SC_6H_{13})_{18}]^x$ collected after 30 min had the charge states of $x = +2, +1, 0, -1$, whereas $[Au_{25}(SC_6H_{13})_{18}]^x$ collected after 3 h had only the -1 charge state. Voltammetric measurements confirmed that redox reactions of $Au_{25}(SC_{12}H_{25})_{18}$ proceeded reversibly, whereas those of $Au_{11}(PPh_3)_8Cl_3$ did not. The first (Ox_1) and second (Ox_2) peaks in Figure 5b are redox couples of $-1/0$ and $0/+1$, respectively. The high tolerance of $Au_{25}(SC_{12}H_{25})_{18}$ to the redox reactions is in sharp contrast to phosphine-stabilized AuCLs. Jin used single-crystal X-ray diffraction to unambiguously demonstrate that the charge state of $Au_{25}(SC_2H_4Ph)_{18}$ could be converted from -1 to 0 by air oxidation.[71] These results lead us to conclude that the electronic structure is not directly responsible for the magic stability of Au:SR clusters.

Regarding the geometric structures of magic Au:SR clusters, the thiolates had long been thought to bind to the bridged or hollow sites on the facets of the highly symmetric Au nanocrystals[72–75] based on the time-honored structural model for the self-assembled monolayer of thiolates on an extended Au surface. Garzón et al. were the first to point out that thiolate ligation can significantly distort the structure of Au core.[76,77] Häkkinen, Walter, and Grönbeck extended this idea by proposing the "divide-and-protect" concept in which thiolates form cyclic tetramers $–[Au^I–S(R)–]_4$ on the surface of the Au core.[78] Iwasa and Nobusada proposed a "core-in-cage" model

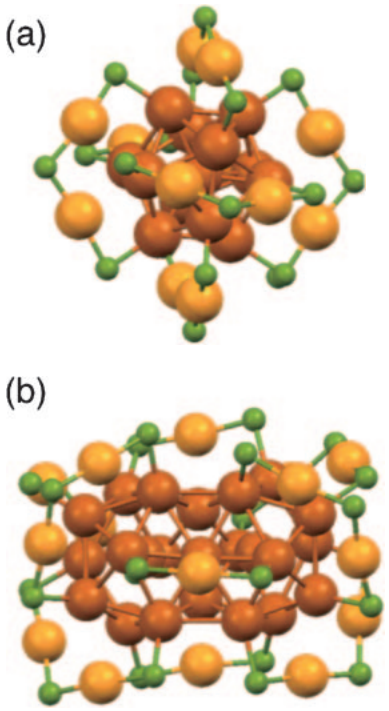

Figure 6. Geometrical structures of (a) $Au_{25}(SR)_{18}$ (Refs. 59 and 60) and (b) $Au_{38}(SR)_{24}$ (Ref. 67). Larger and smaller spheres represent Au and S, respectively. The R groups are omitted for simplicity.

in which the Au core is caged in larger cyclic $–[Au^I–S(R)–]_x$ oligomers.[79] Kornberg's group made a breakthrough in 2007 by elucidating the structure of $Au_{102}(SR)_{44}$ using single-crystal X-ray diffraction.[68] Subsequently, the groups of Murray and Jin experimentally determined the structure of $Au_{25}(SR)_{18}$,[59,60] while Häkkinen et al. theoretically predicted the structure of this cluster (Figure 6a).[80] A recent theoretical prediction for the structure of $Au_{38}(SR)_{24}$ (Refs. 66 and 81–83), namely that it is composed of a face-fused bi-icosahedral Au_{23} core capped by three $–S(R)–[Au–S(R)–]$ and six $–S(R)–[Au–S(R)–]_2$ ligands, was confirmed by a single-crystal X-ray crystallography study

Table 1. Structure Evolution of Magic Au:SR Clusters

Molecular formula		$Au_{25}(SR)_{18}$	$Au_{38}(SR)_{24}$	$Au_{102}(SR)_{44}$
Number of –S(R)–[Au–S(R)–]$_x$	$x = 1$	0	3	19
	$x = 2$	6	6	2
Total number of S anchors		12	18	42[a)]
Size and structures of Au core		Au_{13}	Au_{23}	Au_{79}
Number of surface atoms		12	18	40

a) Forty-two S anchors are adsorbed on the 40 surface atoms by two cases of double anchoring.

by Jin's group (Figure 6b).[67] These reports have dramatically altered the traditional view of the structure of Au:SR clusters: specifically, that $Au_{102}(SR)_{44}$, $Au_{38}(SR)_{24}$, and $Au_{25}(SR)_{18}$ have a common structural motif and consist of two components, Au cluster core and –S(R)–[Au–S(R)–]$_x$ oligomers with different lengths, $n = 1$ and 2. Table 1 summarizes the number of these structural subunits. Based on these common structural features, we proposed the following three principles for building-up magic Au:SR clusters.[43]

(1) The Au cores form highly symmetric and stable geometric structures.

(2) All the surface atoms on the Au core are anchored by thiolates at both ends of –S(R)–[Au–S(R)–]$_x$.

(3) The relative population of longer –S(R)–[Au–S(R)–]$_n$ is higher for smaller clusters because smaller Au cores with larger curvature prefer protection by longer –S(R)–[Au–S(R)–]$_x$, which has a bent structure.

By using principles (1) and (2), the geometric structures of magic clusters such as $Au_{20}(SR)_{16}$,[84,85] $Au_{44}(SR)_{28}$,[86] and $Au_{144}(SR)_{60}$ (Ref. 87) have been predicted theoretically. For example, Häkkinen's group proposed that an Au_{114} core is fully protected by 30 –S(R)–Au–S(R)– staples in the case of $Au_{144}(SR)_{60}$.[87] A longer –S(R)–[Au–S(R)–]$_3$ has been proposed to protect the smaller Au cores of $Au_{20}(SR)_{16}$.[84,85] Figure 7 shows a plot of the populations of Au atoms in the core and –S(R)–[Au–S(R)–]$_x$ oligomers ($x = 1$–3) as a function of the total number of Au atoms. This plot shows that the populations of the core atoms and shorter oligomers increase with increasing number of Au atoms. We recently reanalyzed the ^{197}Au Mössbauer spectrum of $Au_{25}(SG)_{18}$ (Ref. 88) based on the structure model shown in Figure 6a and found that ^{197}Au Mössbauer spectrometry can be used to estimate the relative populations of Au atoms in three different chemical environments, namely in the core mantle, on the core surface, and on the oligomers.[89] The difference in the stability of two Au–S binding modes of $Au_{25}(SG)_{18}$ was probed by NMR spectroscopy.[90]

Once the chemical formula has been determined, these empirical rules can be used to provide an initial estimate for the structural motif of Au:SR clusters. The above discussion leads us to conclude that the magic stability of Au:SR is attributable to both geometric and electronic factors. Namely, the stability

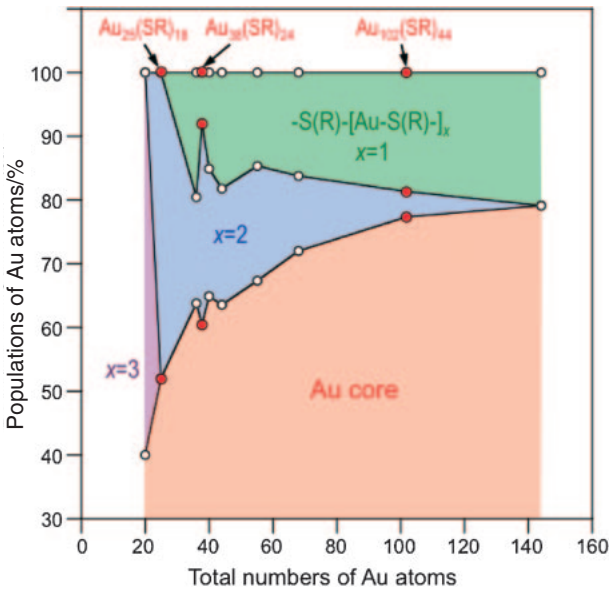

Figure 7. Populations of Au atoms in the core and –S(R)–[Au–S(R)–]$_x$ oligomers in the $Au_n(SR)_m$ compounds reported thus far. Red and white dots represent experimentally determined and proposed populations, respectively.

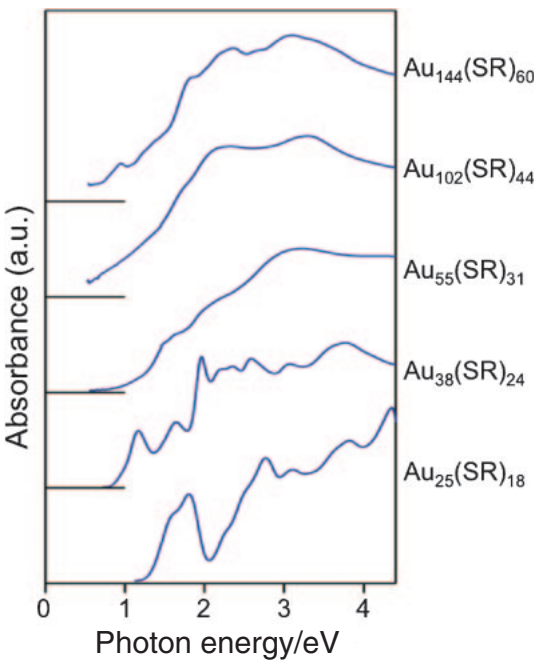

Figure 8. Optical spectra of a series of magic Au:SR clusters.

of magic clusters can be explained in terms of the full protection of highly symmetric Au cores by –S(R)–[Au–S(R)–]$_x$ oligomers and the electronic shell model explains the preferred charge state of each magic cluster.

2.2.3 Physicochemical Properties: 2.2.3.1 Size-Dependent Optical Absorption; As expected, various properties of small Au:SR clusters depend strongly on the cluster size. For example, optical spectra of Au:SR evolve remarkably, as shown in Figure 8.[15,16,28,63] The spectral profiles differ greatly

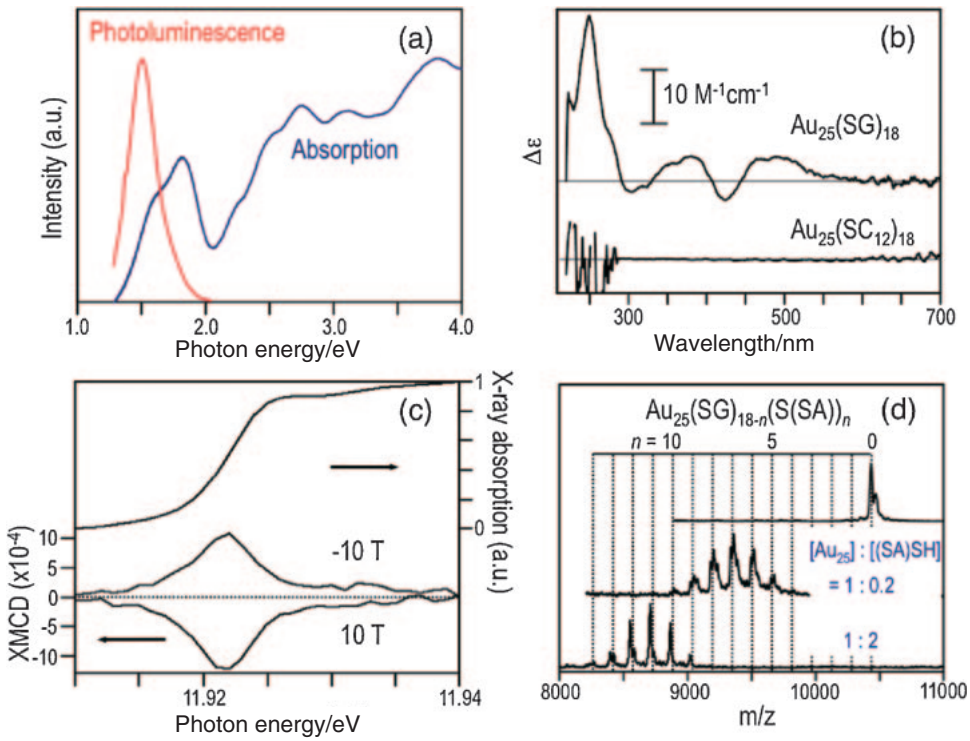

Figure 9. (a) Photoluminescence and absorption spectra of $Au_{25}(SG)_{18}$, (b) CD spectra of $Au_{25}(SG)_{18}$ and $Au_{25}(SC_{12})_{18}$, (c) XMCD of $Au_{25}(SG)_{18}$, and (d) ESI mass spectrum of reaction mixture of $Au_{25}(SG)_{18} + n$(SA)SH.

from those of thiolate-protected AuNPs (>2 nm), which exhibit a surface plasmon band at ca. 2.3 eV on an otherwise smooth profile. Clear absorption onsets are observed below 1.2 eV and they are blue-shifted with decreasing cluster size. This indicates that the HOMO–LUMO gap varies in this size regime. The onsets are followed by various humps and sharp structures. These unique profiles are now regarded as fingerprints of the magic Au:SR clusters; the structures of the head groups (R) have little effect on the electronic structures of Au:SR clusters. These optical properties demonstrate that these Au:SR clusters are better viewed as Au nanomolecules with discrete electronic structures.

2.2.3.2 Novel Properties of $Au_{25}(SR)_{18}$; Au:SR clusters with small cores exhibit novel properties (e.g., optical, photophysical, chiroptical, magnetic, and chemical) that differ from those of the corresponding nanoparticles or bulk material. This section summarizes several interesting properties of Au:SR with a focus on the ubiquitous smallest magic clusters $Au_{25}(SR)_{18}$.

Quantization of the electronic structures of $Au_{25}(SR)_{18}$ leads to interesting optical properties. As mentioned in Section **2.2.3.1**, the optical spectrum exhibits an onset and various other structures. Recent theoretical studies of $Au_{25}(SR)_{18}{}^{-1}$ by Häkkinen and Aikens assigned the first peaks at ≈1.7 eV to optical transitions between sp-based orbitals localized in the Au_{13} core.[80,91–94] Because of the molecular-like electronic structures, $Au_{25}(SR)_{18}$ exhibits photoluminescence (PL) at 1.5 eV (800 nm) with a quantum yield of 1×10^{-3} (Figure 9a).[28] This result is consistent with a previous report by Whetten who initially assigned the compound to $Au_{28}(SR)_{16}$.[95] In addition to this visible PL, they observed another PL band in the near infrared (IR) (1.15 eV, 1100 nm) region with a quantum yield of 2.0×10^{-3}.[95] These PL bands in the visible and IR regions were assigned to the fluorescence and phosphorescence from excited singlet and triplet states, respectively. Although the quantum yields are too low for practical applications, the quantum yields are enhanced by an order of 10^6 relative to that of bulk Au. The effect of ligands and dynamics of the photoexcited states were studied.[96–100] Quantization of the electronic structures is also evidenced by the electrochemical behavior. Cyclic voltammetry of $Au_{25}(SC_{12}H_{25})_{18}$ (Figure 5b) clearly exhibits molecular-like redox properties rather than double-layer charging properties, which is consistent with results obtained by Murray's group.[62] The other important feature is the reversibility of the redox reactions. The high durability of the redox reactions is due to strong Au–SR bonding: it is promising for future applications as components of electronic devices.

Circular dichroism (CD) is another interesting optical property of small Au:SR clusters. Since the first observation by Whetten's group,[26] several studies have investigated the CD properties of AuCLs protected by chiral thiols such as penicillamine and *N*-isobutyrylcysteine.[101–105] Figure 9b shows the CD spectra of $Au_{25}(SC_{12})_{18}$ and $Au_{25}(SG)_{18}$.[106] The $Au_{25}(SG)_{18}$ clusters protected by chiral GS were optically active in the visible and UV spectral ranges with anisotropy factors of the order of several tens to hundred parts per million, which agrees well with the original report by Whetten's group.[26] In contrast, $Au_{25}(SC_{12})_{18}$ clusters protected by achiral dodecanethiolates do not exhibit CD activity. This optical activity is ascribed to the chirality of the GS ligands. The origin of the optical activity in metal-based electronic transitions is still unclear although several models have been proposed.[106–109]

The ferromagnetism of thiolate-protected AuNPs[110,111] has attracted interest recently because bulk Au is diamagnetic. The origin of this magnetism is still being debated. For example, controversial proposals have been made regarding the effect of chemical modification on the magnetism of AuNPs. Crespo et al. have proposed that the magnetism of AuNPs originates from 5d holes localized on Au atoms on the NP surface via charge transfer in Au–S bonds.[110] A theoretical study has predicted the induction of spin polarization of Au_{13} by chemisorption of C_6H_5–X (X = O, S, and Se).[112] In contrast, Hori and co-workers have reported that thiol passivation quenches the spin polarization of surface atoms of AuNPs through electron paring in Au–S bonding.[111] To address this issue, we measured the magnetic moments of a series of $Au_n(SG)_m$ (Ref. 113) by X-ray magnetic circular dichroism (XMCD) which is an element-selective magnetic probe. Figure 9c shows an X-ray absorption spectrum (XAS) and an XMCD spectrum at the Au L_3 edge ($2p_{3/2} \rightarrow 5d_{5/2}$, $6s_{1/2}$) of $Au_{25}(SG)_{18}$ at 2.7 K under a field of 10 T.[113] The XMCD amplitudes were of the order of a thousandth of the XAS step height. The sign of the XMCD signal reversed when the magnetic field was switched to −10 T. These observations verify that the Au atoms in $Au_n(SG)_m$ are inherently spin polarized. The spin-polarization mechanism based on Au(5d) hole created by thiolates ligation was tested by evaluating the magnetic moment per Au–S bond. According to the structural model presented in Section **2.2.2**, the number of Au–S bonds in $Au_n(SG)_m$ is given by $2n$. The magnetic moment per Au–S bond for $Au_n(SG)_m$ were found to be comparable with that of sodium gold thiomalate having a polymer structure with a –Au–S– repeated backbone. We interpreted these results as implying that the spin polarization is due to the Au(5d) hole created by thiolates ligation;[113] the partial electron transfer at the Au–S interface was confirmed by X-ray photoelectron spectroscopy (XPS).[28] Jin's group recently used electron paramagnetic resonance spectroscopy to demonstrate that $Au_{25}(SC_2H_4Ph)_{18}$ possesses one unpaired spin per cluster in the neutral charge state, whereas it is nonmagnetic in the anionic form.[114] Density functional theory calculations indicated that the magnetism observed in $Au_{25}(SC_2H_4Ph)_{18}$ arises from one unpaired spin having a distinct p-like character and being delocalized over the icosahedral Au_{13} core. The highly delocalized spin density is consistent with the superatom picture[70] in which the Au_{13} core possesses a delocalized electronic structure, whereas the outer shell forms strong covalent bonds with the thiolates to protect the particle.

$Au_{25}(SR)_{18}$ clusters exhibit several unique chemical properties that offer various opportunities for applications. We showed in Section **2.2.1** that magic clusters are stable against etching in the presence of excess thiols. However, mass spectrometric analysis revealed that the thiolate exchange reaction proceeds efficiently without alternating the chemical compositions.[115–120] Figure 9d shows a typical ESI mass spectrum of the reaction products of $Au_{25}(SG)_{18}$ and (SA)SH. The products were assigned to $Au_{25}(SG)_{18-n}(S(SA))_n$ and the average number of (SA)S ligands introduced reflected the relative concentration of the incoming SASH and the GS ligands bound to the clusters. This indicates that the ligand exchange proceeds while preserving the chemical composition. Although the details of the mechanism are not clear, this process is useful for functionalizing Au_{25} clusters with thiols having tailored properties.[115] Catalysis is another surprising chemical property of $Au_{25}(SR)_{18}$. It is generally thought that thiolates poison Au catalysts because of their high affinity for Au, which causes them to have high coverages on Au. Jin's group has demonstrated that $Au_{25}(SG)_{18}$ acts as a chemoselective catalyst for oxidation of styrene and hydrogenation of α,β-unsaturated ketones (or aldehydes) to unsaturated alcohols.[121,122] Recently, synthesis of 25-atom alloy clusters with well-defined compositions, such as $Au_{24}Pd(SC_2H_4Ph)_{18}$,[123] $Au_{24}Pd(SC_n)_{18}$,[124] $Au_{25-n}Ag_n(SC_n)_{18}$,[125] has been reported by Murray's and Negishi's group. These clusters were selectively prepared by coreduction of the corresponding metal precursor ions followed by purification. Selective introduction of a single Pd atom is probably associated with its preferred location at the center of the Au_{13} core.[124] Interestingly, Murray demonstrated that titration of metal ions ($M = Ag^+$, Cu^{2+}, or Pb^{2+}) with $[Au_{25}(SC_2H_4Ph)_{18}]^-$ in CH_2Cl_2 replaced Au atoms with M.[126] They proposed a reaction model in which $[Au_{25}(SC_2H_4Ph)_{18}]^-$ acts as a reductant to the metal ion, forming $Au_{25}M(SC_2H_4Ph)_{18}$ adducts that become oxidatively dissociated during the mass spectral cationization to yield bimetallic products.

2.3 Phosphine-Protected Au Clusters. 2.3.1 Bi-icosahedral Au_{25} Clusters $[Au_{25}(PPh_3)_{10}(SC_2H_5)_5Cl_2]^{2+}$: We serendipitously obtained a single crystal of $[Au_{25}(PPh_3)_{10}(SC_2H_5)_5Cl_2]^{2+}$ with two SbF_6^- counter anions in the reaction of $[Au_{11}(PPh_3)_8Cl_2]^+$ with C_2H_5SH (reaction 3).[24] Its chemical identity was confirmed by positive-ion ESI mass spectrometry. Figure 10a shows a schematic diagram of the core framework of $[Au_{25}(PPh_3)_{10}(SC_2H_5)_5Cl_2]^{2+}$ as determined by single-crystal XRD analysis; carbon and hydrogen atoms are omitted for clarity. Interestingly, the Au_{25} core forms a dimer of Au_{13} icosahedrons connected by a single vertex Au atom, which is in contrast to the face-fused bi-icosahedral Au_{23} core of $Au_{38}(SR)_{24}$ (Figure 6b). Ten PPh_3 ligands coordinate on top of peripheral Au atoms. Five ethanethiolates bridge Au_5 pentagon rings of two Au_{13} icosahedrons and two chlorides coordinate to two apical Au atoms. As in the case of magic Au:SR clusters, the ligands completely passivate all the surface Au atoms.

The vertex-sharing bi-icosahedral structure of the Au_{25} core of $[Au_{25}(PPh_3)_{10}(SC_2H_5)_5Cl_2]^{2+}$ is reminiscent of a series of mixed-metal 25-atom cluster compounds, such as $[Au_{13}Ag_{12}(PR_3)_{10}Cl_7]^{2+}$ which have been extensively studied by Teo and co-workers (Figure 10b).[127] The structure of $[Au_{25}(PPh_3)_{10}(SC_2H_5)_5Cl_2]^{2+}$ can be constructed from $[Au_{13}Ag_{12}(PR_3)_{10}Cl_7]^{2+}$ by replacing the Ag and bridging Cl atoms with Au atoms and thiolates, respectively. Successful isolation of monometallic Au_{25} cluster is attributable to the bonding nature of the thiolates, which have a high affinity for Au and prefer to bridge two Au atoms. The stability of these bi-icosahedrons has been explained by the electron counting rule developed by Mingos based on the jellium model; the total number of valence electrons is $8n_p$, where n_p represents the number of icosahedrons.[128] For example, the total number of valence electrons of $[Au_{13}Ag_{12}(PR_3)_{10}Cl_7]^{2+}$ ($n_p = 2$) is calculated to be 16, indicating that $[Au_{13}Ag_{12}(PR_3)_{10}Cl_7]^{2+}$ can be regarded as a dimer of closed-shell, eight-electron systems. Based on these geometric and electronic considerations, Teo has categorized these clusters into "clusters of clusters"

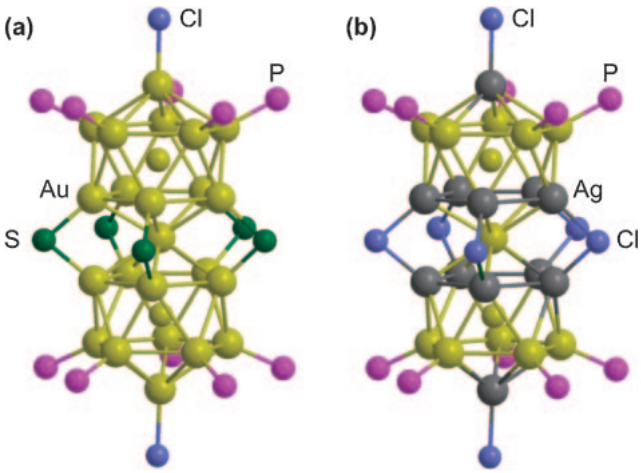

Figure 10. Geometrical structures of (a) $[Au_{25}(PPh_3)_{10}(SC_2H_5)_5Cl_2]^{2+}$ and (b) $[Au_{13}Ag_{12}(PR_3)_{10}Cl_7]^{2+}$. The R groups are omitted for simplicity.

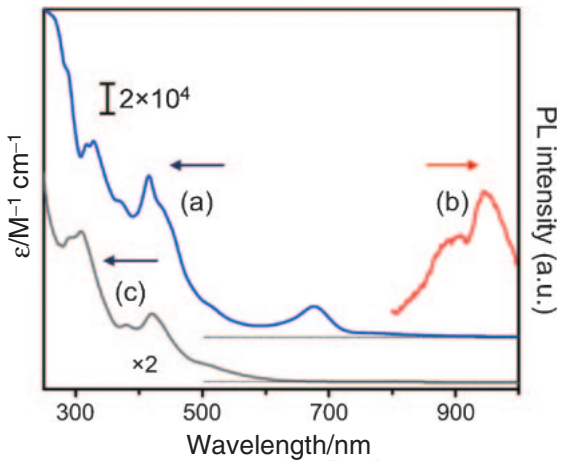

Figure 11. (a) Optical absorption and (b) photoluminescence spectra of $[Au_{25}(PPh_3)_{10}(SC_2H_5)_5Cl_2]^{2+}$ in ethanol. The absorption spectrum of (c) $[Au_{11}(PPh_3)_8Cl_2]^{+}$ in chloroform is shown for comparison.

in which individual icosahedrons serve as the basic building units.[127] The total number of valence electrons in $[Au_{25}(PPh_3)_{10}(SC_2H_5)_5Cl_2]^{2+}$ has been calculated to be 16, which satisfies the above-mentioned electron counting rule.

Optical spectroscopy reveals that the interaction between the two Au_{13} sites is sufficiently strong to create new molecular orbitals, but weak enough to retain the individual properties. Figure 11 shows the optical absorption spectrum of $[Au_{25}(PPh_3)_{10}(SC_2H_5)_5Cl_2]^{2+}$ and $[Au_{11}(PPh_3)_8Cl_2]^{+}$.[24] At wavelengths <500 nm, the spectral profile of $[Au_{25}(PPh_3)_{10}(SC_2H_5)_5Cl_2]^{2+}$ is very similar to that of $[Au_{11}(PPh_3)_8Cl_2]^{+}$, whereas a peak at 670 nm is observed only for $[Au_{25}(PPh_3)_{10}(SC_2H_5)_5Cl_2]^{2+}$. The emergent absorption peak is a direct consequence of dimerization of the Au_{13} units as supported by a recent theoretical study by Nobusada and Iwasa.[129] This absorption has been assigned to the optical transition from the HOMO to the LUMO, which are localized within five atoms of the central axis. The observed PL (yield ≈10%) is also a consequence of dimerization. On the other hand, the spectral

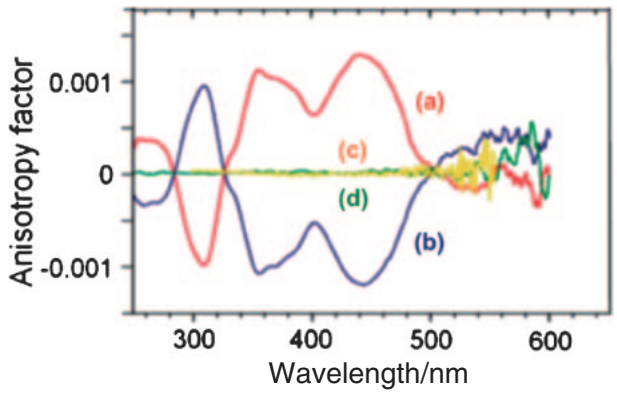

Figure 12. Anisotropy factors of (a) $[Au_{11}(R\text{-BINAP})_4Br_2]^{+}$, (b) $[Au_{11}(S\text{-BINAP})_4Br_2]^{+}$, (c) $Au_{11}(PTMB)_7Cl_3$, and (d) $[Au_{11}(PPh_3)_8Cl_2]^{+}$.

profile in the wavelength range <500 nm is similar to those of $[Au_{25}(PPh_3)_{10}(SC_2H_5)_5Cl_2]^{2+}$ and $[Au_{13}(PMe_2Ph)_{10}Cl_2]^{3+}$ and is thus assigned to optical transitions localized within the Au_{13} moieties. In other words, the intrinsic nature of the individual Au_{13} sites is preserved even though they share a vertex atom. A recent time-resolved spectroscopic study by Jin's group revealed that a photoexcited state of $[Au_{25}(PPh_3)_{10}(SC_2H_5)_5Cl_2]^{2+}$ relaxes via a rapid internal conversion process (0.8 ps) from the LUMO+n to the LUMO, which is followed by a slow relaxation (2.37 μs) to the ground state.[130] The Au_{25} cluster can be viewed as the smallest entity of cluster-assembled materials, in which new optical properties also occur due to the interaction between two Au_{13} icosahedrons. An interesting experimental challenge is to produce higher orders of poly-icosahedrons predicted by Nobusada and Jiang.[129,131]

2.3.2 Chiral Au_{11} Clusters $[Au_{11}(BINAP)_4Br_2]^{2+}$: We utilized 2,2′-bis(diphenylphosphino)-1,1′-binaphthyl (BINAP), a bidentate phosphine ligand with axial chirality, to protect AuCLs.[23] Undecagold cluster compounds $[Au_{11}(BINAP)_4X_2]^{+}$ (X = Cl or Br) were obtained by chemical reduction of the corresponding precursor complexes, $Au_2X_2(BINAP)$ (reaction 2). Although $[Au_{11}(BINAP)_4X_2]^{+}$ and $[Au_{11}(PPh_3)_8Cl_2]^{+}$ clusters contain the same numbers of Au, phosphine, and halogen atoms, the former clusters are much more robust due to bidentate ligation.[132–134] In the framework of the structural model for $[Au_{11}(PPh_3)_8Cl_2]^{+}$, it is reasonable to assume that eight Au atoms are bound to four BINAP ligands and the two remaining Au sites are capped by halogens in $[Au_{11}(BINAP)_4X_2]^{+}$. Recent density functional theory calculations by Aikens predict a chiral structure with C_2 symmetry for $Au_{11}L_4X_2^{+}$ (where L is BINAP or 1,4-diphosphino-1,3-butadiene).[135] The high stability and abundance of these Au_{11}^{3+} cores are well accounted for by the electron counting scheme of Mingos (8 e),[136] Pyykkö (18 e),[137] and Häkkinen (8 e).[70]

We observed that the ligand chirality dramatically affects the CD spectra of Au_{11}^{3+} clusters. Figure 12 shows CD spectra of $[Au_{11}(R\text{-BINAP})_4Br_2]^{+}$, $[Au_{11}(S\text{-BINAP})_4Br_2]^{+}$, $Au_{11}(PTMB)_7Cl_3$, and $[Au_{11}(PPh_3)_8Cl_2]^{+}$, where PTMB represents 4,4′,4″-phosphinidyne-tris(*N*-methylbenzamide). The ordinates in Figure 12 represents the anisotropy factor ($\Delta e/e$). The CD spectra of $[Au_{11}(R\text{-BINAP})_4Br_2]^{+}$ and $[Au_{11}(S\text{-BINAP})_4Br_2]^{+}$ exhibit intense Cotton effects and a

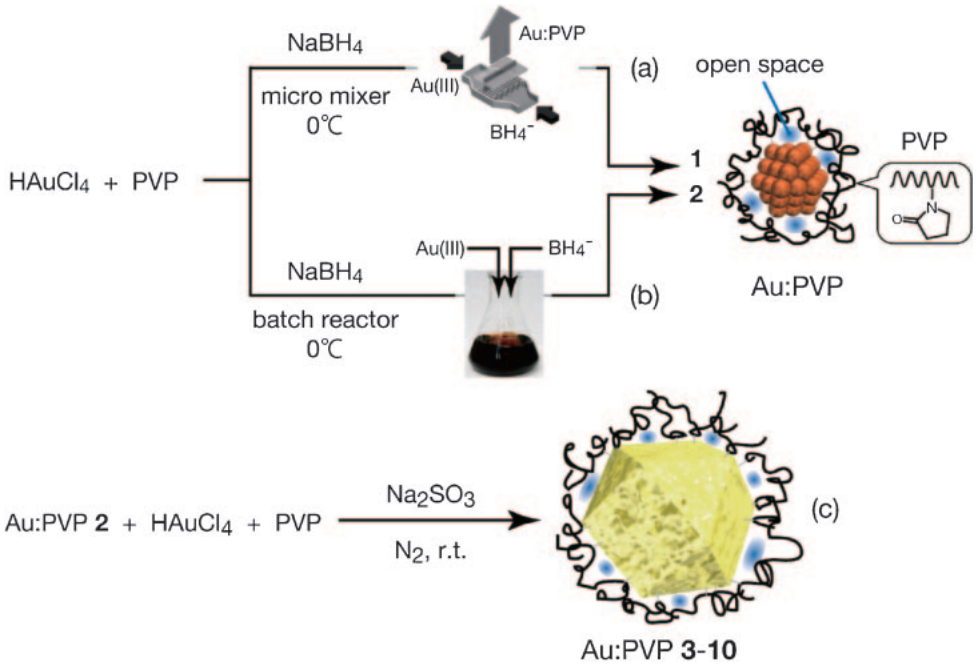

Figure 13. Synthesis of Au:PVP-n ($n = 1$–10).

mirror-image relationship in the 250–500 nm range, whereas $Au_{11}(PTMB)_7Cl_3$ and $[Au_{11}(PPh_3)_8Cl_2]^+$ protected by achiral ligands are not optically active. The optical activity of $[Au_{11}(R\text{-BINAP})_4Br_2]^+$ and $[Au_{11}(S\text{-BINAP})_4Br_2]^+$ observed in the 250–500 nm range is associated with the optical transitions localized within the Au_{11}^{3+} core. Aikens proposed that the optical activity is due to chiral core structure of Au_{11}^{3+} as well as chiral arrangement of the surrounding ligands.[135]

3. Polymer-Stabilized Au Clusters

3.1 Size-Controlled Synthesis. Generally, MNPs are prepared by aggregation of metal atoms produced by chemical reduction of the corresponding metal ions. According to classical nucleation theory,[138] the formation of MNPs proceeds in three steps; nucleation, growth, and aging. In the nucleation step, tiny nuclei are spontaneously formed from supersaturated metal precursor atoms. Nucleation terminates when the precursor metal atoms concentration falls below a critical concentration, but growth continues. In most cases, nucleation and growth occur concurrently throughout MNP formation, so that the final MNPs exhibit a broad size distribution. Thus, to prepare small MCLs with a narrow size distribution, all the precursor ions should be instantaneously and homogeneously reduced over the reaction vessel. These requirements can be fulfilled by using a micromixer and a strong reducing agent such as $NaBH_4$.

3.2 PVP-Stabilized Au Clusters (Au:PVP). 3.2.1 Synthesis and Characterization: Poly(*N*-vinyl-2-pyrrolidone) (PVP), which is a representative stabilizer of colloidal MNPs, was used to stabilize AuCLs.[139–142] A series of Au:PVP was prepared by the method depicted in Figure 13.[143–146] First, small Au:PVP clusters with diameters of ≈1 nm were prepared by rapid reduction of $HAuCl_4$ by a strong reducing agent $NaBH_4$ in the presence of PVP in water.

$$[Au^{III}Cl_4]^- + PVP \xrightarrow{NaBH_4} Au^0{:}PVP \quad (6)$$

The two solutions were mixed by microfluidic mixing (route a)[146] or conventional batch mixing (route b).[143–145] By overlaying laminated substreams with a thickness of 70 μm, the microfluidic mixer mixes the two solutions more homogeneously than is possible by batch mixing. Au:PVP with diameters of 1.1 ± 0.2 (Au:PVP-1) and 1.3 ± 0.3 nm (Au:PVP-2) were obtained by microfluidic and batch mixing, respectively (Figure 13). The significantly improved size distribution obtained using the micromixer is attributed to rapid homogeneous mixing[147] of the $HAuCl_4$ and $NaBH_4$ solutions. X-ray diffraction, extended X-ray absorption fine structure, and MALDI-MS analyses revealed that Au:PVP-1 has a smaller average diameter than Au:PVP-2.[146,148] Figure 14 shows representative MALDI mass spectra of Au:PVP-1 and Au:PVP-2 in the negative-ion mode.[149] A series of naked Au cluster anions, Au_n^-, was observed in the mass spectra. Au:PVP-2 contained more Au_n^- ions with $n > 70$ than Au:PVP-1, which is consistent with the results obtained by other methods. The populations of magic clusters with sizes of 35, 43, 58, 70, 107, 130, and 150 were remarkably enhanced by increasing the synthesis temperature to 40 °C.[149] Magic numbers smaller than ≈70 agree with those of free clusters and can be qualitatively explained by the electronic shell model.[3–6] In contrast, magic numbers larger than ≈100 clearly differ from those of the free clusters. We suggest that the deviation from the electronic shell model is due to perturbation of the electronic and/or geometric structures caused by interaction with PVP. Au:PVP clusters with diameters larger than 2 nm were prepared by a seed-mediated growth method (route c).[145] In this method, a weak reducing agent, Na_2SO_3, is used to reduce additional Au(III) precursor ions only on the surface of seed AuCLs.

$$Au^0{:}PVP + [Au^{III}Cl_4]^- \xrightarrow{Na_2SO_3} Au^0{:}PVP \quad (7)$$

A series of Au:PVP with diameters in the range 2–10 nm was obtained for different concentration ratios of Au(III)/Au(0).

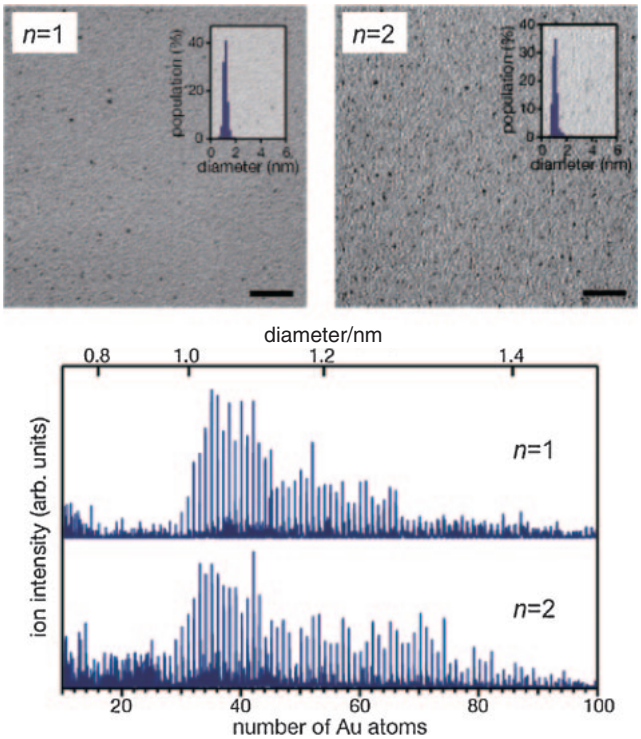

Figure 14. Typical TEM images of Au:PVP-*n* ($n = 1$ and 2): scale bars represent 20 nm. MALDI mass spectra of Au:PVP-*n* ($n = 1$ and 2) in negative-ion mode.

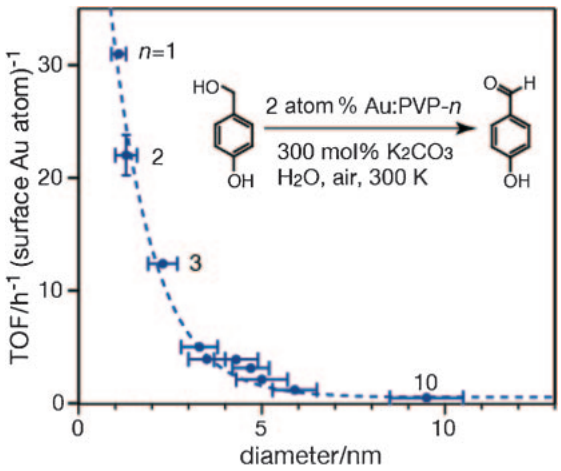

Figure 15. TOF values of Au:PVP-*n* for aerobic oxidation of *p*-hydroxybenzyl alcohol as a function of cluster diameter. The dotted curve is a guide for the eye.

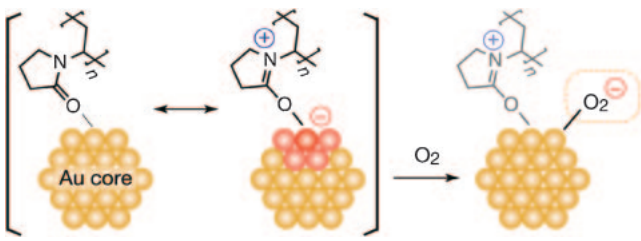

Figure 16. Catalytic activation of O_2 by Au:PVP-*n* for aerobic oxidation of *p*-hydroxybenzyl alcohol.

The clusters obtained are denoted by Au:PVP-*n* ($n = 3$–10) in the order of their cluster size, d_{av}.

3.2.2 Catalysis for Aerobic Oxidation of Alcohols: Au:PVP-2 acts as a catalyst for various aerobic oxidation reactions,[150–155] including oxidation of alcohols. All these reactions proceed under air or O_2, but are completely suppressed under inert gas.

The effect of cluster size on oxidation catalysis was studied using oxidation of *p*-hydroxybenzyl alcohol as a test reaction since *p*-hydroxybenzaldehyde was selectively obtained and Au:PVP-*n* did not aggregate during this reaction.[144,145] The activities of all Au:PVP-*n* clusters were estimated from the pseudo-first-order rate constant obtained from the time course of *p*-hydroxybenzaldehyde production. The turnover frequency (TOF) was obtained by normalizing the rate constants by the number of surface atoms and was then plotted (Figure 15); the TOF increases dramatically when the diameter decreases below 2 nm.[144,145,148] Similar size dependences have been observed in other aerobic oxidation reactions, including H_2O_2 generation from ammonium formate and oxidative homocoupling of arylborates.[150,151]

To determine the origin of the size-specific catalysis of Au:PVP-*n*, we studied the electronic structures of the Au cores using X-ray absorption near-edge spectroscopy (XANES), Fourier-transform infrared (FTIR) spectroscopy of adsorbed CO molecules, and XPS.[148] The intensity of white line at the Au L_3 edge in the XANES spectra of Au:PVP-*n* decreased with decreasing cluster size. This observation indicates that small, active Au:PVP-*n* has a lower d-hole density than bulk Au. The vibrational peak of CO adsorbed on Au:PVP-*n* was red-shifted with decreasing cluster size. This trend is similar to that observed in the FTIR spectra of CO adsorbed on free Au_n^-, which has been qualitatively explained by efficient electron transfer from Au_n^- to the LUMO (π^*) of CO.[156] The smallest, active Au:PVP-1 and -2 had comparable ν_{CO} frequencies as the negative Au site,[157,158] which indicates that the Au core is negatively charged. The dependence of the ν_{CO} frequencies on the PVP concentration indicates that excess PVP donate electrons to the Au core. The Au 4f band of Au:PVP-1 (82.7 eV) is lower than that of bulk Au (84.0 eV). These results clearly indicate that PVP donates an electronic charge to the Au core, probably through interaction with –N–C=O groups (Figure 16). Recent theoretical calculations also suggest that an electron is transferred from the pyrrolidone group to the Au_{13} core.[159] Based on the above observations, we propose the following mechanism for aerobic oxidation catalysis: the Au core is negatively charged by electron donation from PVP and the electrons deposited on the high-lying molecular orbitals of the smaller clusters are transferred to O_2 molecules to form superoxo or peroxo-like species, which may abstract the α-hydrogen of the alcohol (Figure 16). This model is supported by the enhancement of catalysis by silver doping[160] and the suppression of catalysis when stabilized by poly(arylamine), which donates less electronic charge than PVP.[148]

3.3 Star Polymer-Stabilized Au Clusters (Au:EOEOVE). AuCLs show promise as aerobic oxidation catalysts, but several problems need to be resolved before they can be used in practical applications. First, the AuCLs should be robust so that

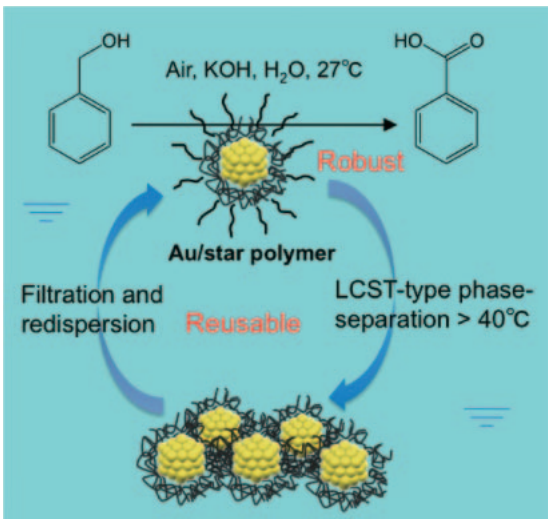

Figure 17. Aerobic oxidation of benzyl alcohol by Au:star(EOEOVE).

they can be recycled; a growth of AuCLs was observed during some oxidation reactions for Au:PVP and recovering Au:PVP by ultrafiltration is time consuming. Aoshima and co-workers overcame these problems by using a unimolecular micellar polymer, star(EOEOVE), as a scaffold for preventing aggregation.[161] Au:star(EOEOVE) clusters could be dispersed in water at temperatures below 40 °C and they oxidized benzyl alcohol into benzoic acid. Au:star(EOEOVE) clusters were precipitated above 40 °C due to star(EOEOVE) having a lower critical solution temperature for phase separation in water (Figure 17). The Au:star(EOEOVE) clusters could be reused at least six times with no loss of activity.

4. Solid-Supported Au Clusters

4.1 Size-Controlled Synthesis. Synthesis of supported AuCLs with atomically controlled sizes is technically challenging since conventional methods can tune only the *average* diameter. To overcome this difficulty, colloidal AuNPs and phosphine-protected AuCLs have been used as precursors.[162–167] Monodisperse Au catalysts have recently been obtained by calcinating monodisperse AuCLs protected by thiolates[166,167] and $Au_{55}(PPh_3)_{12}Cl_6$ (Ref. 162) on metal oxides. We applied this approach to synthesize size-selected cluster catalysts using a series of ligand-protected AuCLs with precisely defined sizes, including Au_{11}:PR_3, $Au_{25}(SR)_{18}$, $Au_{38}(SR)_{24}$, $Au_{55}(SR)_{31}$, and $Au_{144}(SR)_{60}$. Our method consists of two steps: ligand-protected AuCLs with a well-defined size are adsorbed on the surface of solid supports and the ligands are then removed by calcination while suppressing agglomeration (Figure 18). It is very important to reduce the density of precursor clusters to suppress aggregation of AuCLs by using a support with a high surface area.[168]

4.2 Au Clusters Supported on Mesoporous Silica (Au/SBA-15). 4.2.1 Synthesis and Characterization: Using the approach described in Section **4.1**, we prepared a series of size-selected AuCLs with average diameters smaller than 2 nm on pure silica supports with a mesoporous structure (SBA-15, HMS, and MCF).[169,170] First, Au_{11}^{3+} magic clusters

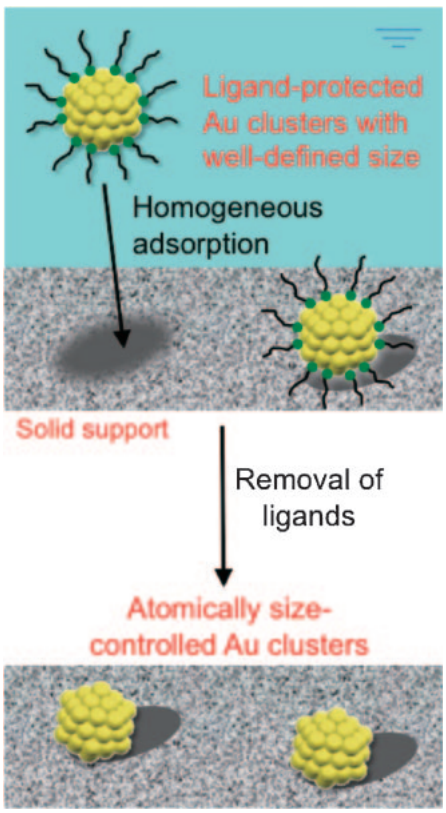

Figure 18. Scheme of size-controlled synthesis of AuCLs on a solid.

(diameter: 0.8 nm), protected by triphenylphosphine (Au_{11}:PPh_3), were deposited on SBA-15 (0.16 wt %) in a mixture of C_2H_5OH and CH_2Cl_2. The BET surface area and average pore size of SBA-15 used in the present study were ≈900 $m^2\,g^{-1}$ and 8.0 nm, respectively. The $0.16Au_{11}$:PPh_3/SBA composite was then calcined to remove the ligands while suppressing the aggregation of the resulting AuCLs. Thermogravimetric analysis of Au_{11}:PPh_3 revealed that calcination at 200 °C for 2 h in vacuum removes all the ligands from the Au_{11} core.[169] Scanning transmission electron microscopy (STEM) observations and small-angle XRD measurements revealed that the calcination did not affect the structure of the SBA-15 support. Larger AuCLs were prepared by controlling the calcination time; the Au_{11}:PPh_3 clusters aggregate to form larger clusters within SBA-15 during prolonged calcination.[170] Calcination for 2, 8, and 16 h yielded $0.16Au_{11}$/SBA(2), $0.16Au_{11}$/SBA(8), and $0.16Au_{11}$/SBA(16), respectively; the Au loading was 0.16 wt % with respect to the substrate.

The cluster size was evaluated by high-angle annular dark-field STEM (HAADF-STEM) and diffuse reflectance UV–vis spectroscopy. Figure 19 shows HAADF-STEM images and the size distributions of the AuCLs. By measuring the diameters of more than 200 particles from the three samples, the average diameters were determined to be 0.8 ± 0.3, 1.5 ± 0.6, and 1.9 ± 1.0 nm for $0.16Au_{11}$/SBA(2), $0.16Au_{11}$/SBA(8), and $0.16Au_{11}$/SBA(16), respectively. The average diameter of 0.8 ± 0.3 nm is comparable to that of PPh_3-protected Au_{11} precursors. The surface plasmon band of the AuCLs is absent for $0.16Au_{11}$/SBA(2), but it becomes pronounced with

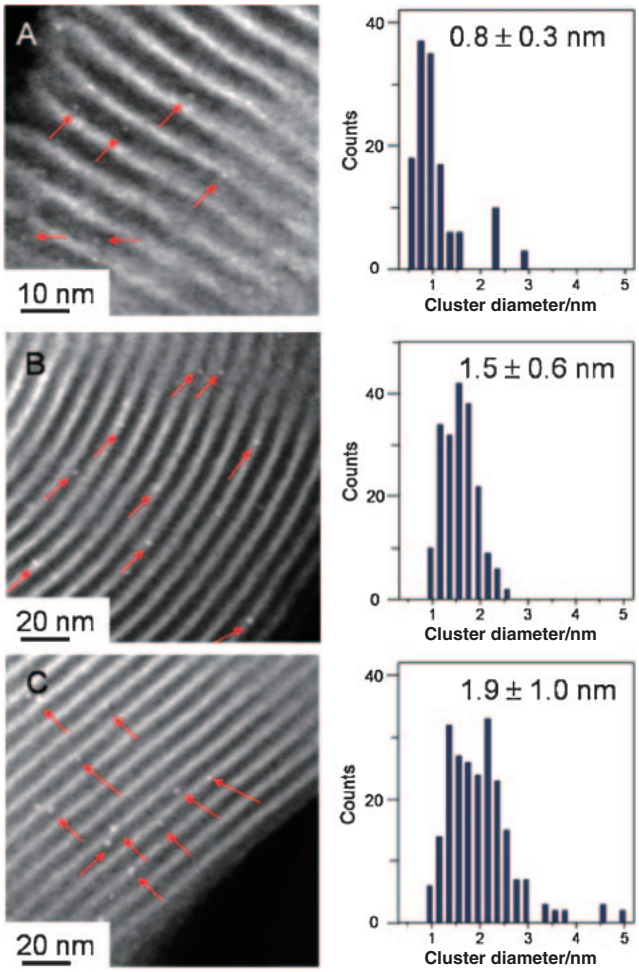

Figure 19. HAADF-STEM images and size distributions of AuCLs in (a) $0.16Au_{11}$/SBA(2), (b) $0.16Au_{11}$/SBA(8), and (c) $0.16Au_{11}$/SBA(16).

increasing calcination time. This trend is consistent with the HAADF-STEM results and indicates that Au_{11} clusters aggregate into larger particles due to the thermal-induced migration of Au_{11} clusters in $0.16Au_{11}$/SBA(8) and $0.16Au_{11}$/SBA(16). On the other hand, the Au_{11} clusters remain intact in $0.16Au_{11}$/SBA(2) due to the smaller possibility of aggregation during migration for a shorter calcination time.

4.2.2 Catalysis for Microwave-Assisted Oxidation of Benzyl Alcohol: The effect of cluster size on the activity of AuCLs on silica was studied by using oxidation of benzyl alcohol as a test reaction.[169,170] In this study, H_2O_2 was used as the oxidant and the reaction was conducted at 60 °C since the catalytic efficiency was too low under aerobic conditions and at ambient temperature. Microwave heating was essential to promote the reaction, probably because it causes superheating. The AuCLs are probably heated directly by the microwave radiation. Benzoic acid and benzaldehyde were obtained as major and minor products, respectively. The highest conversion rate (100%) was obtained for the smallest (0.8 nm) AuCLs and the conversion rate decreased to 81 and 32% for 1.5 and 1.9 nm clusters, respectively. This result demonstrates that even AuCLs supported on inert silica can catalyze oxidation reactions when the cluster size is sufficiently small.

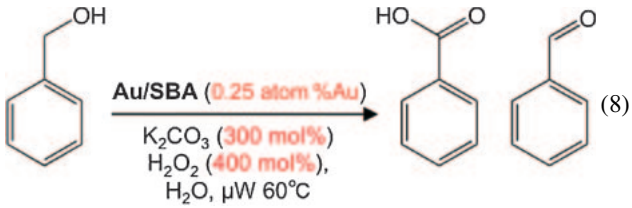

(8)

4.3 Au Clusters Supported on Hydroxyapatite (Au/HAP). 4.3.1 Synthesis and Characterization: A series of size-controlled Au_n clusters on $Ca_{10}(PO_4)_6(OH)_2$ (HAP) was synthesized in two steps (Figure 18) by using size-selected $Au_n(SG)_m$ as a precursor.[171,172] HAP was selected as a support for AuCLs[173–175] since it was expected to adsorb $Au_n(SG)_m$ as efficiently as other biomolecules via hydrogen bonding and/or the electrostatic interaction[176] and that HAP could stabilize bare Au_n clusters against sintering due to its strong interaction with the PO_4^{3-} moiety.[177] First, $Au_n(SG)_m$ clusters with $(n, m) = (10, 10)$, (18, 14), (25, 18), and (39, 24) were prepared by the method described in Section **2.1** and were adsorbed on HAP (surface area: $\approx 100\,m^2\,g^{-1}$) in basic water (pH ≈9.8). The basic condition was employed to promote deprotonation of the carboxylate moieties of the GS ligands and thereby to make $Au_n(SG)_m$ negatively charged. This allowed $Au_n(SG)_m$ to be homogeneously adsorbed over HAP due to the electrostatic repulsion between them. The composite collected by filtration is referred to as $0.2Au_n(SG)_m$/HAP since the amount of Au loaded was estimated to be 0.2 wt % with respect to that of HAP from the molar extinction coefficient.[28] Optical reflectance spectroscopy measurements and TEM observations indicated that $Au_n(SG)_m$ clusters were adsorbed on HAP with their form intact in $0.2Au_n(SG)_m$/HAP. Then, $0.2Au_n(SG)_m$/HAP was calcined at 300 °C for 2 h in vacuo to obtain $0.2Au_n$/HAP.[172] This calcination condition was employed because thermogravimetric analysis of the $Au_n(SG)_m$ precursors showed that the weight lost under the condition coincides well with the calculated weight of the GS ligands. Effective removal of the GS ligands was confirmed by the absence of sulfur in inductively coupled plasma and XPS analysis of $0.2Au_n$/HAP. TEM observations of $0.2Au_n$/HAP revealed no appreciable aggregation of AuCLs during calcination. Figure 20 shows typical TEM images of $0.2Au_n$/HAP and size distributions for AuCLs obtained by counting more than 250 particles. The average diameters (d_{av}) of the AuCLs in $0.2Au_n$/HAP for $n = 10$, 18, 25, and 39 appeared to lie in the range 1.0–1.1 nm, which is comparable to that of the $Au_n(SG)_m$ precursors, irrespective of the size of the $Au_n(SG)_m$ precursors. Although TEM was unable to differentiate the cluster sizes of the four $0.2Au_n$/HAP samples (as expected based on its spatial resolution), we conclude that aggregation of AuCLs during calcination is negligible. Optical spectra of $0.2Au_n$/HAP have different profiles indicating that the AuCLs of $0.2Au_n$/HAP contain different numbers of atoms.[172] However, close inspection of Figure 20 reveals that morphology of AuCLs is not uniform probably due to the heat-induced structural arrangement and/or the strong interaction between AuCLs and HAP. Although the size of the AuCLs can be controlled in atomic level by the approach shown in Figure 18, it is a challenge to control their geometric structures.

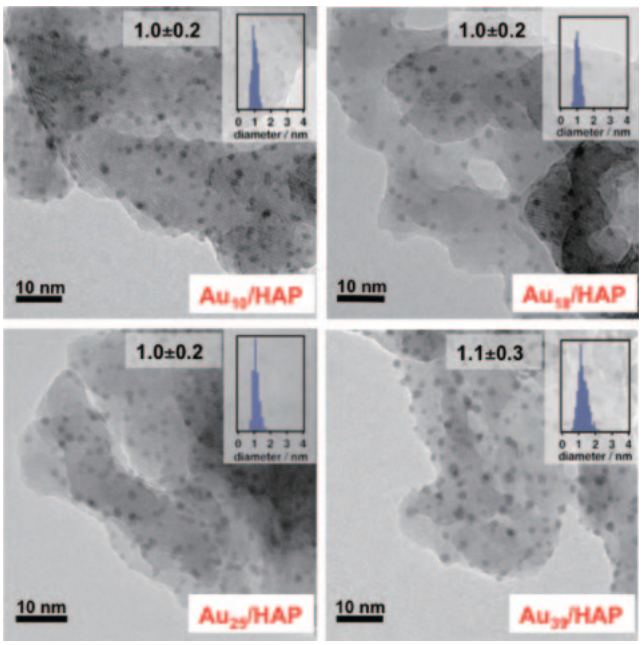

Figure 20. Representative TEM images and size distributions of $0.2Au_n$/HAP ($n = 10$, 18, 25, and 39).

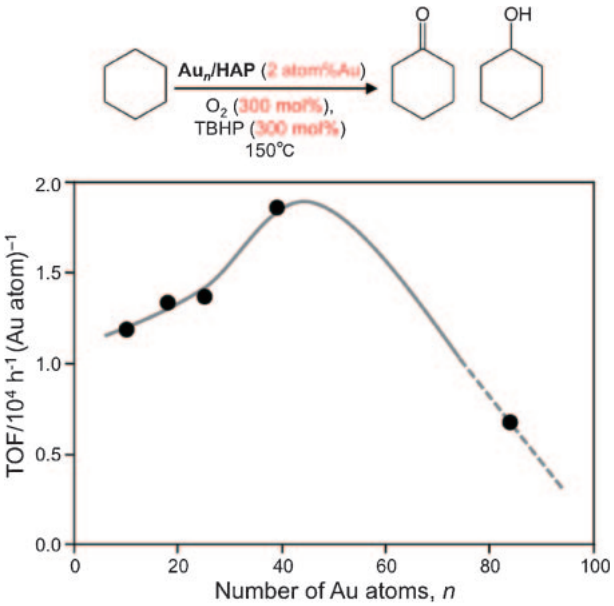

Figure 21. TOF values of $0.2Au_n$/HAP for aerobic oxidation of cyclohexane as a function of cluster size n. The curve is a guide for the eye.

4.3.2 Catalysis for Aerobic Oxidation of Cyclohexane: Aerobic oxidation of cyclohexane is industrially important because its products, cyclohexanone and cyclohexanol (ketone/alcohol or KA–oil), are key intermediates in the production of nylon-6 and nylon-66. However, this reaction is still challenging in modern chemistry due to the chemical inertness of cyclohexane.[178,179] Several groups have recently shown that supported AuNPs ($d_{av} > 3$ nm) have the potential to efficiently catalyze aerobic oxidation of cyclohexane.[180–186] We studied the catalytic performances of $0.2Au_n$/HAP ($n = 10$, 18, 25, and 39) for oxidation of cyclohexane. As a reference, we also used larger and polydisperse AuCLs ($d_{av} = 1.4 \pm 0.6$ nm, 0.2 wt % of Au) on HAP prepared by a conventional adsorption method.[172] The reference catalyst is hereafter referred to as $0.2Au_{\approx 85}$/HAP because the average Au cluster diameter corresponds to that of Au_{85} (assuming that the clusters have the same density as bulk Au). Oxidation of cyclohexane by $0.2Au_n$/HAP under an O_2 atmosphere (1 MPa) and solvent-free conditions at 150 °C yielded cyclohexanol and cyclohexanone as the primary products with nearly equivalent yields; adipic acid was not formed. The addition of a small amount of TBHP ([TBHP]/[cyclohexane] $= 1.2 \times 10^{-3}$) was essential to initiate the reaction,[183] suggesting that this oxidation proceeds via a complex radical chain mechanism.[179,186]

The total selectivities for KA oil were very high and nearly constant regardless of the conversion; the selectivities were as high as ≈99% for smaller $0.2Au_n$/HAP ($n = 10$–39), whereas the selectivity was slightly smaller (≈95%) for $0.2Au_{\approx 85}$/HAP. This is in sharp contrast to the previously reported trade-off relationship between conversion and selectivity[181,185] Figure 21 shows a plot of the TOF values (defined as the number of cyclohexane converted per Au atom in the cluster per hour) as a function of cluster size n. The TOF values increase monotonically with increasing size in the range $n = 10$ to 39, but decrease in the range $n = 39$ to ≈85. Figure 21 reveals that there is an optimal Au cluster size in the range $n = 40$ to 80 for aerobic oxidation of cyclohexane. Although it is not currently clear how the AuCLs participate the complex oxidation processes, the volcano-shaped size dependence in Figure 21 cannot be explained solely in terms of geometric factors such as the surface area and density of low-coordination sites on AuCLs.

$0.2Au_n$/HAP ($n = 10$–39) catalysts exhibit several notable features. First, they had very high catalytic performances: the total selectivities for KA oil and the TOF values are among the highest reported.[180–186] Second, the catalytic performance was highly reproducible; the conversions obtained for three independently synthesized samples of $0.2Au_{25}$/HAP were similar, typically having a standard deviation of less than 1%. Third, they are robust and reusable; $0.2Au_{25}$/HAP catalysts could be reused at least three times with no noticeable loss in activity. This recyclability is ascribed to their durability under the present conditions, as evidenced by optical spectra and TEM images obtained before and after they were used as catalysts.[172]

4.3.3 Catalysis for Epoxidation of Styrene: Since Haruta's group first demonstrated propene epoxidation using molecular oxygen in 1998,[187] supported gold catalysts have been used for the selective epoxidation/oxidation of various alkenes such as styrene, cyclohexene, *cis*-cyclooctene, and *trans*-stilbene.[162,188–193] $0.5Au_{25}$/HAP was found to catalyze selective oxidation of styrene.[171] Oxidation of styrene in toluene at 80 °C using anhydrous TBHP as an oxidant yielded styrene oxide as a major product and acetophenone, benzaldehyde, benzyl alcohol, and benzoic acid were produced as by-products. To our knowledge, this yield of styrene oxide is one of the highest reported to date. It was essential to use toluene as a solvent to obtain styrene oxide in a high yield, in sharp contrast to the case of Au/graphite and Au/SiO_2. The use of anhydrous toluene and TBHP was also important for enhancing the yield of styrene oxide.

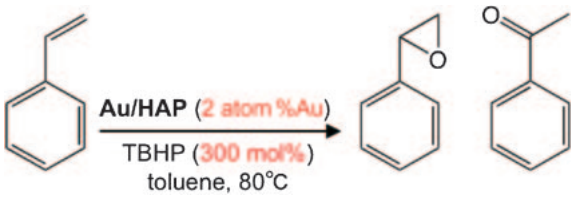

(9)

The catalysis of $0.5Au_{25}$/HAP was compared with other 0.5Au/HAP catalysts with average diameters of 1.7 ± 1.2 and 6.0 ± 3.7 nm prepared by a conventional method.[171] The conversion rate was not strongly dependent on the size, whereas the selectivity of styrene oxide for $0.5Au_{25}$/HAP was 92–95%, which was much higher than those (50–60%) of the reference catalysts. We suggested that the high selectivity of $0.5Au_{25}$/HAP can be explained based on the extremely slow decomposition of styrene oxide by Au_{25} clusters. The $0.5Au_{25}$/HAP also showed excellent reusability without any significant loss in either the catalytic activity or the selectivity of the formation of styrene oxide. Finally, we tested the catalytic activity of $0.5Au_{25}$/HAP against styrene oxidation in toluene in an O_2 atmosphere (1 atm). Microwave heating at 100 °C for 2 h yields styrene oxide with a conversion of 22% and a selectivity of 36% despite the reaction conditions not being optimized.

5. Summary and Prospects

In this study, we aimed to synthesize AuCLs by translating the knowledge obtained using a model system of free AuCLs. This account summarizes the precision synthesis and size-dependent properties of three types of AuCLs protected by ligands (RS and R_3P), stabilized by polymers (PVP and starEOEOVE), and supported on solids (SBA-15 and HAP).

The ligand-protected AuCLs were size-selectively synthesized by fractionation with PAGE/SEC and they were characterized by mass spectrometry. We discovered several magic clusters, such as $Au_{25}(SR)_{18}$, $Au_{38}(SR)_{24}$, $Au_{55}(SR)_{31}$, $Au_{144}(SR)_{60}$, $[Au_{25}(PPh_3)_{10}(SR)_5X_2]^{2+}$, and $[Au_{11}(BINAP)_4X_2]^{2+}$. We proposed a building-up principle for the magic Au:SR clusters using the two components, the Au cluster core, and $–S(R)–[Au–S(R)–]_x$ oligomers ($x = 1$–3). The $[Au_{25}(PPh_3)_{10}(SR)_5X_2]^{2+}$, which consists of two icosahedral Au_{13} clusters, is a stepping stone for cluster-assembled materials. Chirality was induced by ligation with the chiral bidentate ligand, BINAP, in $[Au_{11}(BINAP)_4X_2]^{2+}$.

Size control of the polymer-stabilized AuCLs was achieved by a microfluidic method. MALDI mass analysis revealed the formation of magic AuCLs similar to those in the gas phase. Au:PVP dispersed in water exhibited size-specific catalysis for aerobic oxidation of alcohols. Spectroscopic studies revealed that oxidation catalysis can be explained by activation of molecular oxygen via electron transfer from negatively-charged AuCLs, as has been proposed for free Au cluster anions.

Size-controlled AuCLs were synthesized on the solids by using ligand-protected AuCLs as precursors. These AuCLs show high activity and selectivity in oxidation reactions of styrene and cyclohexane. We demonstrated for the first time that catalysis of gold occurs only in the cluster regime and that there is an optimal size for catalysis.

The precise and systematic method for synthesizing AuCLs that we developed is versatile and highly reproducible. This approach will deepen our fundamental understanding of the structure–property correlation of MCLs at the atomic level and will contribute to the development of cluster-based functional materials. Similarities observed between model and real AuCLs convince us that fundamental knowledge of a model system can be used to develop practical guidelines for designing the cluster-based materials. We hope that the present strategy will open up new opportunities for MCLs in materials science.

The author wishes sincerely thank to all the co-workers whose names appear in the references. This work was supported by Grants-in-Aid (Nos. 21245001 and 21655044) from MEXT, the CREST program of JST, and Funding Program for Next-Generation World-Leading Researchers (NEXT Program) (GR-003). The author thanks Drs. Yuichi Negishi, Hironori Tsunoyama, and Risako Tsunoyama for their help with preparing the manuscript.

References

1 M. Brack, *Rev. Mod. Phys.* **1993**, *65*, 677.
2 A. W. Castleman, Jr., K. H. Bowen, Jr., *J. Phys. Chem.* **1996**, *100*, 12911.
3 K. J. Taylor, C. L. Pettiette-Hall, O. Cheshnovsky, R. E. Smalley, *J. Chem. Phys.* **1992**, *96*, 3319.
4 I. Katakuse, T. Ichihara, Y. Fujita, T. Matsuo, T. Sakurai, H. Matsuda, *Int. J. Mass Spectrom. Ion Processes* **1985**, *67*, 229.
5 J. Li, X. Li, H.-J. Zhai, L.-S. Wang, *Science* **2003**, *299*, 864.
6 H.-J. Zhai, L.-S. Wang, *J. Chem. Phys.* **2005**, *122*, 051101.
7 M. Haruta, T. Kobayashi, H. Sano, N. Yamada, *Chem. Lett.* **1987**, 405.
8 W. T. Wallace, R. L. Whetten, *J. Am. Chem. Soc.* **2002**, *124*, 7499.
9 Y. D. Kim, M. Fischer, G. Ganteför, *Chem. Phys. Lett.* **2003**, *377*, 170.
10 T. M. Bernhardt, *Int. J. Mass Spectrom.* **2005**, *243*, 1.
11 W. Huang, H.-J. Zhai, L.-S. Wang, *J. Am. Chem. Soc.* **2010**, *132*, 4344.
12 L. D. Socaciu, J. Hagen, T. M. Bernhardt, L. Wöste, U. Heiz, H. Häkkinen, U. Landman, *J. Am. Chem. Soc.* **2003**, *125*, 10437.
13 *Nanocatalysis* in *NanoScience and Technology*, ed. by U. Heiz, U. Landman, Springer-Verlag, Berlin, **2007**. doi:10.1007/978-3-540-32646-5.
14 M. Brust, M. Walker, D. Bethell, D. J. Schiffrin, R. Whyman, *J. Chem. Soc., Chem. Commun.* **1994**, 801.
15 R. L. Whetten, J. T. Khoury, M. M. Alvarez, S. Murthy, I. Vezmar, Z. L. Wang, P. W. Stephens, C. L. Cleveland, W. D. Luedtke, U. Landman, *Adv. Mater.* **1996**, *8*, 428.
16 R. L. Whetten, M. N. Shafigullin, J. T. Khoury, T. G. Schaaff, I. Vezmar, M. M. Alvarez, A. Wilkinson, *Acc. Chem. Res.* **1999**, *32*, 397.
17 A. C. Templeton, W. P. Wuelfing, R. W. Murray, *Acc. Chem. Res.* **2000**, *33*, 27.
18 R. Jin, *Nanoscale* **2010**, *2*, 343.
19 G. Schmid, *Chem. Rev.* **1992**, *92*, 1709.
20 L. O. Brown, J. E. Hutchison, *J. Am. Chem. Soc.* **1997**, *119*, 12384.
21 R. Balasubramanian, R. Guo, A. J. Mills, R. W. Murray, *J. Am. Chem. Soc.* **2005**, *127*, 8126.
22 Y. Shichibu, Y. Negishi, T. Tsukuda, T. Teranishi, *J. Am.*

Chem. Soc. **2005**, *127*, 13464.
23 Y. Yanagimoto, Y. Negishi, H. Fujihara, T. Tsukuda, *J. Phys. Chem. B* **2006**, *110*, 11611.
24 Y. Shichibu, Y. Negishi, T. Watanabe, N. K. Chaki, H. Kawaguchi, T. Tsukuda, *J. Phys. Chem. C* **2007**, *111*, 7845.
25 T. G. Schaaff, G. Knight, M. N. Shafigullin, R. F. Borkman, R. L. Whetten, *J. Phys. Chem. B* **1998**, *102*, 10643.
26 T. G. Schaaff, R. L. Whetten, *J. Phys. Chem. B* **2000**, *104*, 2630.
27 Y. Negishi, Y. Takasugi, S. Sato, H. Yao, K. Kimura, T. Tsukuda, *J. Am. Chem. Soc.* **2004**, *126*, 6518.
28 Y. Negishi, K. Nobusada, T. Tsukuda, *J. Am. Chem. Soc.* **2005**, *127*, 5261.
29 Y. Negishi, H. Tsunoyama, Y. Yanagimoto, T. Tsukuda, *Chem. Lett.* **2005**, *34*, 1638.
30 Y. Negishi, Y. Takasugi, S. Sato, H. Yao, K. Kimura, T. Tsukuda, *J. Phys. Chem. B* **2006**, *110*, 12218.
31 K. Kimura, N. Sugimoto, S. Sato, H. Yao, Y. Negishi, T. Tsukuda, *J. Phys. Chem. C* **2009**, *113*, 14076.
32 H. Tsunoyama, Y. Negishi, T. Tsukuda, *J. Am. Chem. Soc.* **2006**, *128*, 6036.
33 H. Tsunoyama, P. Nickut, Y. Negishi, K. Al-Shamery, Y. Matsumoto, T. Tsukuda, *J. Phys. Chem. C* **2007**, *111*, 4153.
34 R. Tsunoyama, H. Tsunoyama, P. Pannopard, J. Limtrakul, T. Tsukuda, *J. Phys. Chem. C* **2010**, *114*, 16004.
35 T. G. Schaaff, R. L. Whetten, *J. Phys. Chem. B* **1999**, *103*, 9394.
36 Y. Negishi, T. Tsukuda, *J. Am. Chem. Soc.* **2003**, *125*, 4046.
37 Y. Negishi, T. Tsukuda, *Chem. Phys. Lett.* **2004**, *383*, 161.
38 T. G. Schaaff, M. N. Shafigullin, J. T. Khoury, I. Vezmar, R. L. Whetten, *J. Phys. Chem. B* **2001**, *105*, 8785.
39 M. Zhu, H. Qian, R. Jin, *J. Am. Chem. Soc.* **2009**, *131*, 7220.
40 M. Zhu, H. Qian, R. Jin, *J. Phys. Chem. Lett.* **2010**, *1*, 1003.
41 J. B. Tracy, G. Kalyuzhny, M. C. Crowe, R. Balasubramanian, J.-P. Choi, R. W. Murray, *J. Am. Chem. Soc.* **2007**, *129*, 6706.
42 Y. Negishi, N. K. Chaki, Y. Shichibu, R. L. Whetten, T. Tsukuda, *J. Am. Chem. Soc.* **2007**, *129*, 11322.
43 N. K. Chaki, Y. Negishi, H. Tsunoyama, Y. Shichibu, T. Tsukuda, *J. Am. Chem. Soc.* **2008**, *130*, 8608.
44 H. Qian, Y. Zhu, R. Jin, *ACS Nano* **2009**, *3*, 3795.
45 H. Qian, Y. Zhu, R. Jin, *J. Am. Chem. Soc.* **2010**, *132*, 4583.
46 H. Qian, R. Jin, *Nano Lett.* **2009**, *9*, 4083.
47 C. A. Fields-Zinna, R. Sardar, C. A. Beasley, R. W. Murray, *J. Am. Chem. Soc.* **2009**, *131*, 16266.
48 Y. Levi-Kalisman, P. D. Jadzinsky, N. Kalisman, H. Tsunoyama, T. Tsukuda, D. A. Bushnell, R. D. Kornberg, *J. Am. Chem. Soc.* **2011**, *133*, 2976.
49 R. C. Price, R. L. Whetten, *J. Am. Chem. Soc.* **2005**, *127*, 13750.
50 A. Dass, A. Stevenson, G. R. Dubay, J. B. Tracy, R. W. Murray, *J. Am. Chem. Soc.* **2008**, *130*, 5940.
51 A. C. Dharmaratne, T. Krick, A. Dass, *J. Am. Chem. Soc.* **2009**, *131*, 13604.
52 A. Dass, *J. Am. Chem. Soc.* **2009**, *131*, 11666.
53 Y. Shichibu, Y. Negishi, H. Tsunoyama, M. Kanehara, T. Teranishi, T. Tsukuda, *Small* **2007**, *3*, 835.
54 R. Jin, H. Qian, Z. Wu, Y. Zhu, M. Zhu, A. Mohanty, N. Garg, *J. Phys. Chem. Lett.* **2010**, *1*, 2903.
55 H. Qian, M. Zhu, E. Lanni, Y. Zhu, M. E. Bier, R. Jin, *J. Phys. Chem. C* **2009**, *113*, 17599.
56 H. Qian, M. Zhu, U. N. Andersen, R. Jin, *J. Phys. Chem. A* **2009**, *113*, 4281.
57 Z. Wu, M. A. MacDonald, J. Chen, P. Zhang, R. Jin, *J. Am. Chem. Soc.* **2011**, *133*, 9670.
58 M. Zhu, E. Lanni, N. Garg, M. E. Bier, R. Jin, *J. Am. Chem. Soc.* **2008**, *130*, 1138.
59 M. W. Heaven, A. Dass, P. S. White, K. M. Holt, R. W. Murray, *J. Am. Chem. Soc.* **2008**, *130*, 3754.
60 M. Zhu, C. M. Aikens, F. J. Hollander, G. C. Schatz, R. Jin, *J. Am. Chem. Soc.* **2008**, *130*, 5883.
61 J. F. Parker, J. E. F. Weaver, F. McCallum, C. A. Fields-Zinna, R. W. Murray, *Langmuir* **2010**, *26*, 13650.
62 J. F. Parker, C. A. Fields-Zinna, R. W. Murray, *Acc. Chem. Res.* **2010**, *43*, 1289.
63 Z. Wu, J. Chen, R. Jin, *Adv. Funct. Mater.* **2011**, *21*, 177.
64 P. R. Nimmala, A. Dass, *J. Am. Chem. Soc.* **2011**, *133*, 9175.
65 S. Knoppe, A. C. Dharmaratne, E. Schreiner, A. Dass, T. Bürgi, *J. Am. Chem. Soc.* **2010**, *132*, 16783.
66 O. Lopez-Acevedo, H. Tsunoyama, T. Tsukuda, H. Häkkinen, C. M. Aikens, *J. Am. Chem. Soc.* **2010**, *132*, 8210.
67 H. Qian, W. T. Eckenhoff, Y. Zhu, T. Pintauer, R. Jin, *J. Am. Chem. Soc.* **2010**, *132*, 8280.
68 P. D. Jadzinsky, G. Calero, C. J. Ackerson, D. A. Bushnell, R. D. Kornberg, *Science* **2007**, *318*, 430.
69 H. Qian, R. Jin, *Chem. Mater.* **2011**, *23*, 2209.
70 M. Walter, J. Akola, O. Lopez-Acevedo, P. D. Jadzinsky, G. Calero, C. J. Ackerson, R. L. Whetten, H. Grönbeck, H. Häkkinen, *Proc. Natl. Acad. Sci. U.S.A.* **2008**, *105*, 9157.
71 M. Zhu, W. T. Eckenhoff, T. Pintauer, R. Jin, *J. Phys. Chem. C* **2008**, *112*, 14221.
72 C. L. Cleveland, U. Landman, T. G. Schaaff, M. N. Shafigullin, P. W. Stephens, R. L. Whetten, *Phys. Rev. Lett.* **1997**, *79*, 1873.
73 H. Häkkinen, R. N. Barnett, U. Landman, *Phys. Rev. Lett.* **1999**, *82*, 3264.
74 W. D. Luedtke, U. Landman, *J. Phys. Chem.* **1996**, *100*, 13323.
75 W. D. Luedtke, U. Landman, *J. Phys. Chem. B* **1998**, *102*, 6566.
76 I. L. Garzón, K. Michaelian, M. R. Beltrán, A. Posada-Amarillas, P. Ordejón, E. Artacho, D. Sánchez-Portal, J. M. Soler, *Phys. Rev. Lett.* **1998**, *81*, 1600.
77 I. L. Garzón, C. Rovira, K. Michaelian, M. R. Beltrán, P. Ordejón, J. Junquera, D. Sánchez-Portal, E. Artacho, J. M. Soler, *Phys. Rev. Lett.* **2000**, *85*, 5250.
78 H. Häkkinen, M. Walter, H. Grönbeck, *J. Phys. Chem. B* **2006**, *110*, 9927.
79 T. Iwasa, K. Nobusada, *J. Phys. Chem. C* **2007**, *111*, 45.
80 J. Akola, M. Walter, R. L. Whetten, H. Häkkinen, H. Grönbeck, *J. Am. Chem. Soc.* **2008**, *130*, 3756.
81 D.-e. Jiang, M. L. Tiago, W. Luo, S. Dai, *J. Am. Chem. Soc.* **2008**, *130*, 2777.
82 Y. Pei, Y. Gao, X. C. Zeng, *J. Am. Chem. Soc.* **2008**, *130*, 7830.
83 D.-e. Jiang, W. Luo, M. L. Tiago, S. Dai, *J. Phys. Chem. C* **2008**, *112*, 13905.
84 D.-e. Jiang, W. Chen, R. L. Whetten, Z. Chen, *J. Phys. Chem. C* **2009**, *113*, 16983.
85 Y. Pei, Y. Gao, N. Shao, X. C. Zeng, *J. Am. Chem. Soc.* **2009**, *131*, 13619.
86 D.-e. Jiang, M. Walter, J. Akola, *J. Phys. Chem. C* **2010**,

114, 15883.
87 O. Lopez-Acevedo, J. Akola, R. L. Whetten, H. Grönbeck, H. Häkkinen, *J. Phys. Chem. C* **2009**, *113*, 5035.
88 K. Ikeda, Y. Kobayashi, Y. Negishi, M. Seto, T. Iwasa, K. Nobusada, T. Tsukuda, N. Kojima, *J. Am. Chem. Soc.* **2007**, *129*, 7230.
89 T. Tsukuda, Y. Negishi, Y. Kobayashi, N. Kojima, *Chem. Lett.* **2011**, *40*, 1292.
90 Z. Wu, R. Jin, *ACS Nano* **2009**, *3*, 2036.
91 C. M. Aikens, *J. Phys. Chem. C* **2008**, *112*, 19797.
92 C. M. Aikens, *J. Phys. Chem. A* **2009**, *113*, 10811.
93 C. M. Aikens, *J. Phys. Chem. Lett.* **2010**, *1*, 2594.
94 C. M. Aikens, *J. Phys. Chem. Lett.* **2011**, *2*, 99.
95 S. Link, A. Beeby, S. FitzGerald, M. A. El-Sayed, T. G. Schaaff, R. L. Whetten, *J. Phys. Chem. B* **2002**, *106*, 3410.
96 Z. Wu, R. Jin, *Nano Lett.* **2010**, *10*, 2568.
97 S. A. Miller, J. M. Womick, J. F. Parker, R. W. Murray, A. M. Moran, *J. Phys. Chem. C* **2009**, *113*, 9440.
98 H. Qian, M. Y. Sfeir, R. Jin, *J. Phys. Chem. C* **2010**, *114*, 19935.
99 S. H. Yau, O. Varnavski, J. D. Gilbertson, B. Chandler, G. Ramakrishna, T. Goodson, III, *J. Phys. Chem. C* **2010**, *114*, 15979.
100 M. S. Devadas, K. Kwak, J.-W. Park, J.-H. Choi, C.-H. Jun, E. Sinn, G. Ramakrishna, D. Lee, *J. Phys. Chem. Lett.* **2010**, *1*, 1497.
101 C. Gautier, T. Bürgi, *J. Am. Chem. Soc.* **2006**, *128*, 11079.
102 H. Yao, T. Fukui, K. Kimura, *J. Phys. Chem. C* **2008**, *112*, 16281.
103 H. Yao, T. Fukui, K. Kimura, *J. Phys. Chem. C* **2007**, *111*, 14968.
104 H. Yao, K. Miki, N. Nishida, A. Sasaki, K. Kimura, *J. Am. Chem. Soc.* **2005**, *127*, 15536.
105 N. Shukla, M. A. Bartel, A. J. Gellman, *J. Am. Chem. Soc.* **2010**, *132*, 8575.
106 T. Tsukuda, H. Tsunoyama, Y. Negishi, in *Metal Nanoclusters in Catalysis and Materials Science: The Issue of Size Control*, ed. by B. Corain, G. Schmid, N. Toshima, Elsevier, **2008**, Chap. 25, pp. 373–382. doi:10.1016/B978-044453057-8.50027-1.
107 C. Noguez, A. Sánchez-Castillo, F. Hidalgo, *J. Phys. Chem. Lett.* **2011**, *2*, 1038.
108 C. Noguez, I. L. Garzón, *Chem. Soc. Rev.* **2009**, *38*, 757.
109 C. E. Román-Velázquez, C. Noguez, I. L. Garzón, *J. Phys. Chem. B* **2003**, *107*, 12035.
110 P. Crespo, R. Litrán, T. C. Rojas, M. Multigner, J. M. de la Fuente, J. C. Sánchez-López, M. A. García, A. Hernando, S. Penadés, A. Fernández, *Phys. Rev. Lett.* **2004**, *93*, 087204.
111 Y. Yamamoto, T. Miura, M. Suzuki, N. Kawamura, H. Miyagawa, T. Nakamura, K. Kobayashi, T. Teranishi, H. Hori, *Phys. Rev. Lett.* **2004**, *93*, 116801.
112 C. Gonzalez, Y. Simón-Manso, M. Marquez, V. Mujica, *J. Phys. Chem. B* **2006**, *110*, 687.
113 Y. Negishi, H. Tsunoyama, M. Suzuki, N. Kawamura, M. M. Matsushita, K. Maruyama, T. Sugawara, T. Yokoyama, T. Tsukuda, *J. Am. Chem. Soc.* **2006**, *128*, 12034.
114 M. Zhu, C. M. Aikens, M. P. Hendrich, R. Gupta, H. Qian, G. C. Schatz, R. Jin, *J. Am. Chem. Soc.* **2009**, *131*, 2490.
115 E. S. Shibu, M. A. Habeeb Muhammed, T. Tsukuda, T. Pradeep, *J. Phys. Chem. C* **2008**, *112*, 12168.
116 J. B. Tracy, M. C. Crowe, J. F. Parker, O. Hampe, C. A. Fields-Zinna, A. Dass, R. W. Murray, *J. Am. Chem. Soc.* **2007**, *129*, 16209.
117 A. Dass, K. Holt, J. F. Parker, S. W. Feldberg, R. W. Murray, *J. Phys. Chem. C* **2008**, *112*, 20276.
118 C. A. Fields-Zinna, J. S. Sampson, M. C. Crowe, J. B. Tracy, J. F. Parker, A. M. deNey, D. C. Muddiman, R. W. Murray, *J. Am. Chem. Soc.* **2009**, *131*, 13844.
119 C. A. Fields-Zinna, J. F. Parker, R. W. Murray, *J. Am. Chem. Soc.* **2010**, *132*, 17193.
120 J. F. Parker, K. A. Kacprzak, O. Lopez-Acevedo, H. Häkkinen, R. W. Murray, *J. Phys. Chem. C* **2010**, *114*, 8276.
121 Y. Zhu, H. Qian, B. A. Drake, R. Jin, *Angew. Chem., Int. Ed.* **2010**, *49*, 1295.
122 Y. Zhu, H. Qian, R. Jin, *J. Mater. Chem.* **2011**, *21*, 6793.
123 C. A. Fields-Zinna, M. C. Crowe, A. Dass, J. E. F. Weaver, R. W. Murray, *Langmuir* **2009**, *25*, 7704.
124 Y. Negishi, W. Kurashige, Y. Niihori, T. Iwasa, K. Nobusada, *Phys. Chem. Chem. Phys.* **2010**, *12*, 6219.
125 Y. Negishi, T. Iwai, M. Ide, *Chem. Commun.* **2010**, *46*, 4713.
126 J.-P. Choi, C. A. Fields-Zinna, R. L. Stiles, R. Balasubramanian, A. D. Douglas, M. C. Crowe, R. W. Murray, *J. Phys. Chem. C* **2010**, *114*, 15890.
127 B. K. Teo, H. Zhang, *Inorg. Chem.* **1991**, *30*, 3115.
128 Z. Lin, R. P. F. Kanters, D. M. P. Mingos, *Inorg. Chem.* **1991**, *30*, 91.
129 K. Nobusada, T. Iwasa, *J. Phys. Chem. C* **2007**, *111*, 14279.
130 M. Y. Sfeir, H. Qian, K. Nobusada, R. Jin, *J. Phys. Chem. C* **2011**, *115*, 6200.
131 D.-e. Jiang, K. Nobusada, W. Luo, R. L. Whetten, *ACS Nano* **2009**, *3*, 2351.
132 M. F. Bertino, Z.-M. Sun, R. Zhang, L.-S. Wang, *J. Phys. Chem. B* **2006**, *110*, 21416.
133 J. S. Golightly, L. Gao, A. W. Castleman, Jr., D. E. Bergeron, J. W. Hudgens, R. J. Magyar, C. A. Gonzalez, *J. Phys. Chem. C* **2007**, *111*, 14625.
134 Y. Shichibu, K. Konishi, *Small* **2010**, *6*, 1216.
135 M. R. Provorse, C. M. Aikens, *J. Am. Chem. Soc.* **2010**, *132*, 1302.
136 D. M. P. Mingos, *Chem. Soc. Rev.* **1986**, *15*, 31.
137 P. Pyykkö, *Angew. Chem., Int. Ed.* **2004**, *43*, 4412.
138 V. K. La Mer, *Ind. Eng. Chem.* **1952**, *44*, 1270.
139 T. Teranishi, M. Miyake, *Chem. Mater.* **1998**, *10*, 594.
140 T. Yonezawa, N. Toshima, in *Advanced Functional Molecules and Polymers: Processing and Spectroscopy*, ed. by H. S. Nalwa, OPA, Amsterdam, **2001**, Vol. 2, p. 65.
141 R. Narayanan, M. A. El-Sayed, *J. Phys. Chem. B* **2005**, *109*, 12663.
142 Y. Zhang, M. E. Grass, J. N. Kuhn, F. Tao, S. E. Habas, W. Huang, P. Yang, G. A. Somorjai, *J. Am. Chem. Soc.* **2008**, *130*, 5868.
143 H. Tsunoyama, H. Sakurai, N. Ichikuni, Y. Negishi, T. Tsukuda, *Langmuir* **2004**, *20*, 11293.
144 H. Tsunoyama, H. Sakurai, Y. Negishi, T. Tsukuda, *J. Am. Chem. Soc.* **2005**, *127*, 9374.
145 H. Tsunoyama, H. Sakurai, T. Tsukuda, *Chem. Phys. Lett.* **2006**, *429*, 528.
146 H. Tsunoyama, N. Ichikuni, T. Tsukuda, *Langmuir* **2008**, *24*, 11327.
147 A. Abou-Hassan, O. Sandre, V. Cabuil, *Angew. Chem., Int. Ed.* **2010**, *49*, 6268.
148 H. Tsunoyama, N. Ichikuni, H. Sakurai, T. Tsukuda, *J. Am. Chem. Soc.* **2009**, *131*, 7086.
149 H. Tsunoyama, T. Tsukuda, *J. Am. Chem. Soc.* **2009**, *131*, 18216.

150 H. Sakurai, H. Tsunoyama, T. Tsukuda, *Trans. Mater. Res. Soc. Jpn.* **2006**, *31*, 521.
151 H. Sakurai, H. Tsunoyama, T. Tsukuda, *J. Organomet. Chem.* **2007**, *692*, 368.
152 H. Tsunoyama, T. Tsukuda, H. Sakurai, *Chem. Lett.* **2007**, *36*, 212.
153 I. Kamiya, H. Tsunoyama, T. Tsukuda, H. Sakurai, *Chem. Lett.* **2007**, *36*, 646.
154 H. Sakurai, I. Kamiya, H. Kitahara, H. Tsunoyama, T. Tsukuda, *Synlett* **2009**, 245.
155 T. Tsukuda, H. Tsunoyama, H. Sakurai, *Chem.—Asian J.* **2011**, *6*, 736.
156 A. Fielicke, G. von Helden, G. Meijer, D. B. Pedersen, B. Simard, D. M. Rayner, *J. Am. Chem. Soc.* **2005**, *127*, 8416.
157 M. Chen, Y. Cai, Z. Yan, D. W. Goodman, *J. Am. Chem. Soc.* **2006**, *128*, 6341.
158 H.-J. Freund, *Catal. Today* **2006**, *117*, 6.
159 M. Okumura, Y. Kitagawa, T. Kawakami, M. Haruta, *Chem. Phys. Lett.* **2008**, *459*, 133.
160 N. K. Chaki, H. Tsunoyama, Y. Negishi, H. Sakurai, T. Tsukuda, *J. Phys. Chem. C* **2007**, *111*, 4885.
161 S. Kanaoka, N. Yagi, Y. Fukuyama, S. Aoshima, H. Tsunoyama, T. Tsukuda, H. Sakurai, *J. Am. Chem. Soc.* **2007**, *129*, 12060.
162 M. Turner, V. B. Golovko, O. P. H. Vaughan, P. Abdulkin, A. Berenguer-Murcia, M. S. Tikhov, B. F. G. Johnson, R. M. Lambert, *Nature* **2008**, *454*, 981.
163 A. I. Kozlov, A. P. Kozlova, H. Liu, Y. Iwasawa, *Appl. Catal., A* **1999**, *182*, 9.
164 J.-D. Grunwaldt, C. Kiener, C. Wögerbauer, A. Baiker, *J. Catal.* **1999**, *181*, 223.
165 T. V. Choudhary, C. Sivadinarayana, C. C. Chusuei, A. K. Datye, J. P. Fackler, Jr., D. W. Goodman, *J. Catal.* **2002**, *207*, 247.
166 Y. Tai, J. Murakami, K. Tajiri, F. Ohashi, M. Daté, S. Tsubota, *Appl. Catal., A* **2004**, *268*, 183.
167 N. Zheng, G. D. Stucky, *J. Am. Chem. Soc.* **2006**, *128*, 14278.
168 T. Matsumoto, P. Nickut, T. Sawada, H. Tsunoyama, K. Watanabe, T. Tsukuda, K. Al-Shamery, Y. Matsumoto, *Surf. Sci.* **2007**, *601*, 5121.
169 Y. Liu, H. Tsunoyama, T. Akita, T. Tsukuda, *J. Phys. Chem. C* **2009**, *113*, 13457.
170 Y. Liu, H. Tsunoyama, T. Akita, T. Tsukuda, *Chem. Lett.* **2010**, *39*, 159.
171 Y. Liu, H. Tsunoyama, T. Akita, T. Tsukuda, *Chem. Commun.* **2010**, *46*, 550.
172 Y. Liu, H. Tsunoyama, T. Akita, S. Xie, T. Tsukuda, *ACS Catal.* **2011**, *1*, 2.
173 A. Venugopal, M. S. Scurrell, *Appl. Catal., A* **2003**, *245*, 137.
174 M. I. Domínguez, F. Romero-Sarria, M. A. Centeno, J. A. Odriozola, *Appl. Catal., B* **2009**, *87*, 245.
175 T. Mitsudome, A. Noujima, T. Mizugaki, K. Jitsukawa, K. Kaneda, *Chem. Commun.* **2009**, 5302.
176 Q. Luo, J. D. Andrade, *J. Colloid Interface Sci.* **1998**, *200*, 104.
177 W. Yan, S. Brown, Z. Pan, S. M. Mahurin, S. H. Overbury, S. Dai, *Angew. Chem., Int. Ed.* **2006**, *45*, 3614.
178 R. Raja, G. Sankar, J. M. Thomas, *J. Am. Chem. Soc.* **1999**, *121*, 11926.
179 U. Schuchardt, D. Cardoso, R. Sercheli, R. Pereira, R. S. da Curz, M. C. Guerreiro, D. Mandelli, E. V. Spinacé, E. L. Pires, *Appl. Catal., A* **2001**, *211*, 1.
180 R. Zhao, D. Ji, G. Lv, G. Qian, L. Yan, X. Wang, J. Suo, *Chem. Commun.* **2004**, 904.
181 G. Lü, R. Zhao, G. Qian, Y. Qi, X. Wang, J. Suo, *Catal. Lett.* **2004**, *97*, 115.
182 K. Zhu, J. Hu, R. Richards, *Catal. Lett.* **2005**, *100*, 195.
183 Y.-J. Xu, P. Landon, D. Enache, A. F. Carley, M. W. Roberts, G. J. Hutchings, *Catal. Lett.* **2005**, *101*, 175.
184 L.-X. Xu, C.-H. He, M.-Q. Zhu, S. Fang, *Catal. Lett.* **2007**, *114*, 202.
185 L.-X. Xu, C.-H. He, M.-Q. Zhu, K.-J. Wu, Y.-L. Lai, *Catal. Lett.* **2007**, *118*, 248.
186 B. P. C. Hereijgers, B. M. Weckhuysen, *J. Catal.* **2010**, *270*, 16.
187 T. Hayashi, K. Tanaka, M. Haruta, *J. Catal.* **1998**, *178*, 566.
188 A. S. K. Hashmi, G. J. Hutchings, *Angew. Chem., Int. Ed.* **2006**, *45*, 7896.
189 C. D. Pina, E. Falletta, L. Prati, M. Rossi, *Chem. Soc. Rev.* **2008**, *37*, 2077.
190 M. D. Hughes, Y.-J. Xu, P. Jenkins, P. McMorn, P. Landon, D. I. Enache, A. F. Carley, G. A. Attard, G. J. Hutchings, F. King, E. H. Stitt, P. Johnston, K. Griffin, C. J. Kiely, *Nature* **2005**, *437*, 1132.
191 D. Gajan, K. Guillois, P. Delichère, J.-M. Basset, J.-P. Candy, V. Caps, C. Coperet, A. Lesage, L. Emsley, *J. Am. Chem. Soc.* **2009**, *131*, 14667.
192 N. S. Patil, B. S. Uphade, P. Jana, S. K. Bharagava, V. R. Choudhary, *J. Catal.* **2004**, *223*, 236.
193 L. Luo, N. Yu, R. Tan, Y. Jin, D. Yin, D. Yin, *Catal. Lett.* **2009**, *130*, 489.

Tatsuya Tsukuda received his Ph.D. degree in chemistry from the University of Tokyo under the supervision of Prof. Tamotsu Kondow in 1994. After postdoctoral research under the guidance of at RIKEN, he was appointed as an Assistant Professor in the Department of Basic Sciences at the University of Tokyo in 1994. He then was appointed as an Associate Professor at Institute for Molecular Science in 2000 and promoted to Professor in Catalysis Research Center at Hokkaido University in 2007. His research interests include size-selected synthesis of metal clusters protected by ligands and solid supports, and their catalytic application.